ISTANBUL TECHNICAL UNIVERSITY ★ GRADUATE SCHOOL

BUCKLING BEHAVIOR OF PLASTICALLY STRAINED METALLIC PANELS

M.Sc. THESIS

Taha ÇİMEN

Department of Mechanical Engineering

Solid Mechanics Engineering Programme

JULY 2025

ISTANBUL TECHNICAL UNIVERSITY ★ GRADUATE SCHOOL

BUCKLING BEHAVIOR OF PLASTICALLY STRAINED METALLIC PANELS

M.Sc. THESIS

Taha ÇİMEN
(503221512)

Department of Mechanical Engineering

Solid Mechanics Engineering Programme

Thesis Advisor: Prof. Dr. Ata MUĞAN

JULY 2025

ISTANBUL TEKNİK ÜNİVERSİTESİ ★ LİSANSÜSTÜ EĞİTİM ENSTİTÜSÜ

PLASTİK GERİNİME UĞRAMIŞ METAL PANELLERİN BURKULMA DAVRANIŞI

YÜKSEK LİSANS TEZİ

Taha ÇİMEN
(503221512)

Makina Mühendisliği Ana Bilim Dalı
Katı Cisimler Mekaniği Programı

Tez Danışmanı: Prof. Dr. Ata MUĞAN

TEMMUZ 2025

Taha Çimen, a M.Sc. student of ITU Graduate School student ID 503221512 successfully defended the thesis/dissertation entitled “BUCKLING BEHAVIOR OF PLASTICALLY STRAINED METALLIC PANELS”, which he prepared after fulfilling the requirements specified in the associated legislations, before the jury whose signatures are below.

Thesis Advisor:	**Prof. Dr. Ata MUĞAN** İstanbul Technical University	.....
Jury Members:	**Prof. Dr. Ekrem TÜFEKCİ** Istanbul Technical University	.....
	Prof. Dr. Hasan YILDIZ Ege University	.....

Date of Submission : 30 May 2025
Date of Defense : 02 July 2025

To my family,

FOREWORD

Completing this thesis is an important step for my academic and professional career. Buckling Behavior of Plastically Strained Metal Panels was selected as the thesis topic due to my strong interest in understanding the behavior of structures under shear load, especially in the fields of aerospace and mechanical engineering.

This thesis was completed with the support and encouragement of many people. First of all, I would like to express my sincere gratitude to my advisor, Prof. Dr. Ata Muğan, for his continuous support and valuable advice throughout the entire process. I am grateful for his excellent guidance and decent contributions.

I would like to thank Prof. Dr. Mustafa Bakkal for providing the tools and resources needed to perform the experimental study. In addition, I sincerely appreciate RMC Engineering Company for supplying the test measurement devices and assisting with their application.

I am thankful to my family and friends for their helpful suggestions and motivation during challenging times. I also wish to express my gratitude to my grandfather, Ali Seçkin, for his understanding and continuous encouragement throughout my studies.

This thesis is the result of detailed research, many revisions, and a strong passion for learning more about structural mechanics. I hope the results and discussions in this work will be useful to others interested in post-buckling behavior.

July 2025 Taha ÇİMEN

TABLE OF CONTENTS

Page

ABBREVIATIONS

FEM	: Finite Element Method
FE	: Finite Element
NACA	: National Advisory Committee for Aeronautics
LCM	: Load Control Method
DCM	: Displacement Control Method
AL	: Aluminum
ST	: Steel
DOF	: Degree of Freedom
DAQ	: Data Acquisition
FEA	: Finite Element Analysis
N	: Newton
kN	: Kilonewton

SYMBOLS

E	**:** Elastic Modulus
υ	: Poisson Ratio
t	: Thickness
k_s	: Shear Buckling Coefficient
L	: Length of Panel
W	: Width of Panel
β	: Slenderness Ratio
σ_Y	: Yield Stress
σ_U	: Tensile Stress
F_U^{LIT}	: Ultimate Buckling Load from Literature
F_U^{FEM}	: Ultimate Buckling Load from FEM
F_{CR}^{LIT}	: Critical Buckling Load from Literature
F_{CR}^{FEM}	: Critical Buckling Load from FEM
r(u)	: Nodal Force Vector
f	: Applied Load Vector
t	: State
Δt	: Interval of State
Δr	: Nodal Force Change
Δu	: Displacement Change
K	: Stiffness Matrix
K_t	: Tangent Stiffness Matrix
ψ	: Arc-Length Scheme Parameter
s	: Arc-Length Parameter
F_{cr}	: Critical Buckling Load
F_u	: Ultimate Buckling Load
με	: Microstrain
u_x	: Translation -X Direction
u_y	: Translation -Y Direction
u_z	: Translation -Z Direction
θ_x	: Rotation -X Direction

θ_y : Rotation -Y Direction

θ_z : Rotation -Z Direction

LIST OF TABLES

Page

LIST OF FIGURES

Page

BUCKLING BEHAVIOR OF PLASTICALLY STRAINED METALLIC PANELS

SUMMARY

During the post-buckling stage, plastic strain can be occurred due to unexpected service loads, which alters the stiffness of the panel and affects their buckling resistance. However, the extent of this reduction and its impact on structural performance have not been thoroughly studied. The objective of this thesis is to investigate the effect of plastic strain on the critical buckling load of panels under in-plane shear loading.

To achieve this, both experimental and numerical analyses were conducted. In the experimental study, an AL-1050 alloy square panel with 330 mm side length and 1 mm thickness of was utilized using a picture frame test setup. Two strain gauges were mounted in a back-to-back on the panel to measure both elastic and plastic strains during loading

For the numerical study, finite element simulations were performed in Abaqus to evaluate the effect of different levels of plastic strain (25%, 50%, 75% and 100%) on the secondary buckling load. These plastic strain levels were taken from the post-buckling condition at the ultimate buckling load, and used as predefined inputs to recalculate the buckling loads.

A total of 18 panel models were created using AL-5754 and ST-37 materials for the numerical study. For each material, panels were modelled with side lengths of 500 mm, 750 mm, and 1000 mm, and thicknesses of 2 mm, 3 mm, and 4 mm.

The aim of the study is to compare the initial critical buckling loads with the secondary buckling loads calculated under different levels of plastic strain, and to identify a relationship between the reduction percentage and the dimension of the panel. The findings contribute to a deeper understanding of buckling behavior in plastically strained metallic panels and provide important insights for the design and safety of load-bearing structures in engineering applications.

PLASTİK GERİNMEYE UĞRAMIŞ METAL PANELLERDE BURKULMA DAVRANIŞI

ÖZET

Panel burkulmasıyla ilgili çalışmalar 1800'lü yıllarda başlamış; Navier, Saint Venant, Bryan ve Timoshenko gibi öncüler, burkulma problemlerine çeşitli teorik yaklaşımlar geliştirmiştir. Bu teoriler, panelin kenar şartlarına, yükleme durumlarına ve geometriye göre burkulma yüklerinin hesaplanmasını amaçlamıştır. 1950'lerde NACA tarafından yayımlanan Gerard ve Becker'in raporu, eğri panellerin elastik ve elastik olmayan burkulma davranışlarını inceleyen kapsamlı bir kaynak olmuştur. Bu çalışmada deneysel veriler ile teorik modeller arasındaki farklar da tartışılmıştır. Birçok araştırma, kesme ve eksenel yük gibi birleşik yüklemelere maruz kalan panellerin burkulma davranışlarına odaklanmıştır. Daha yeni çalışmalarda Kang, Leissa ve Xiang gibi isimler, panellerin burkulma yüklerini farklı sınır koşulları ve oranlar altında daha kesin yöntemlerle hesaplamışlardır.

Burkulma sonrası davranış ise özellikle havacılık yapılarında, yapısal dayanımın optimize edilmesi ve kullanım ömrünün uzatılması açısından önemli bir araştırma alanı olmuştur. Alinia ve Amani gibi araştırmacılar, farklı malzemelerden yapılan düz panellerin burkulma sonrası tepkilerini ve ilk kusurların etkisini incelemişlerdir. Ghadami ve Broujerdian, kusurların etkisini dikkate alan bir yük azaltma katsayısı önererek literatüre katkı sunmuşlardır. Ljubinković, Amani, Park ve Melcon gibi araştırmacılar; eğrilik ve oranların, burkulma ve burkulma sonrası davranış üzerindeki etkilerini incelemiş, bu panellerin özellikle kesme ve basma yükleri altındaki davranışlarını analiz etmişlerdir.

Yalnızca düz veya eğik paneller değil; kafes kirişler, burkulma önleyici takviyeli paneller de kapsamlı şekilde araştırılmıştır. Geleneksel burkulma teorileriyle deneysel sonuçlar karşılaştırılmış, farklı malzemeden yapılmış panellerin nihai taşıma kapasitelerini FEM modelleriyle analiz etmiş ve farklı kesitler kullanılarak yeni tasarım önerileri geliştirmiştir. Bunun yanı sıra takviyelerin burkulma dayanımını nasıl artırdığını ve yük dağılımına olan katkılarını hem deneysel hem sayısal yöntemlerle ortaya koymuşlardır. Bu çalışmalarda, takviye şekli, yönü ve malzeme özelliklerinin önemli rol oynadığı gösterilmiştir.

Tüm bu yapılan çalışmaların yanında metal panellerin burkulma sonrası davranışı sırasında öngörülemeyen servis yüklerine maruz kalabilirler. Bu hesaba katılmayan yükler panelin sertliğini ve burkulma direncini etkileyecek şekilde plastik gerinme oluşturabilir. Ancak oluşan bu sertlik değişimi, burkulma direncindeki değişim ve metal panellerin yapısal performansının nasıl etkilendiği mevcut literatürde yeterince kapsamlı bir şekilde incelenmemiştir. Bu tezin amacı, burkulma sonrası aşamada oluşan plastik gerinmenin, düzlem içi kesme yüküne maruz kalan panellerin kritik burkulma yükü üzerindeki etkisini araştırmaktır.

Bu kapsamda, plastik gerinmenin etkilerini değerlendirmek üzere hem deneysel çalışmalar hem de sonlu elemanlar analizleri yapılmıştır. Deneysel çalışma

kapsamında numune olarak 330 mm kenar uzunluğuna ve 1 mm kalınlığa sahip AL-1050 alaşımlı kare panel kullanılmıştır. Panelin kenarlarında düzlem içi dönmeleri ve düzlem dışı deformasyonları önlemek amacıyla, yükleme resim çerçevesi test düzeneği kullanılarak gerçekleştirilmiştir. Yükleme sırasında hem elastik hem de plastik gerilmeleri ölçmek için panele sırt sırta olacak şekilde iki adet rozet tipi gerinim ölçer yerleştirilmiştir. Gerinim bilgisini ölçmek için DEWESOFT marka veri toplama cihazı kullanılmıştır.

Yapılan test sonucunda elde edilen veriler, geliştirilen sonlu eleman modeli sonuçları ile karşılaştırılmış ve yüksek uyum gösterdiği tespit edilmiştir. Kritik burkulma yükleri ve gerinim değerlerinde %2–6 aralığında düşük hata oranları elde edilmiştir. Bu durum, modelin farklı malzemeler ve geometrik özellikler için güvenle kullanılabileceğini göstermektedir.

Deneysel çalışmalara ek olarak, plastik gerinmenin burkulma yükü üzerindeki etkisini daha kapsamlı analiz edebilmek adına ABAQUS yazılımı kullanılarak sonlu elemanlar analizleri gerçekleştirilmiştir. Sayısal analizlerde farklı malzeme türleri (AL-5754 ve ST-37) ve farklı panel boyutları (kenar uzunlukları 500 mm, 750 mm ve 1000 mm; kalınlıkları 2 mm, 3 mm ve 4 mm) göz önünde bulundurularak toplam 18 farklı model oluşturulmuştur.

Öncelikle her bir model için Lanczos metodu lineer burkulma yükü hesaplanmıştır. Bu analizde elde edilen birinci mod şekli burkulma sonrası analizlerinde kusur olarak tanımlanmıştır. Ardından Statik Riks yöntemi kullanılarak panellerin burkulma sonrası davranışları hesaplanmıştır. Bu adıma kadar yapılan hesaplar literatürde sıkça karşılaşılan hesaplamalardır.

Burkulma sonrası analizlerde hesaplanan plastik gerinme seviyelerinin %25, %50, %75 ve %100'i başlangıç sınır koşulu olarak tanımlanmıştır. Lineer burkulma hesabında kullanılan Lanczos metot ile ikincil burkulma yükleri hesaplanmıştır. Hesaplanan bu değerler kendi aralarında, farklı malzemeler için ve hiç plastik gerinmenin olmadığı durumlar için karşılaştırılmıştır.

Sonuçlar incelendiğinde açıkça plastik gerinim artışının ikincil burkulma yükünü azaltıcı yönde etki ettiği açıkça görünmektedir. Bu etki, yüksek narinlik oranlarına ve düşük kalınlıklara sahip panellerde daha belirgin hale gelirken, kalın ve kısa paneller için burkulma dayanımlarının yüksek oranda korunduğu sonuçlar ile göz önüne serilmiştir.

Farklı malzemeler karşılaştırıldığında, elastisite modülü yüksek malzemeden yapılmış (ST-37) paneller plastik gerinime karşı direnç açısından elastisite modülü düşük malzemeden (AL-5754) yapılmış panellerden daha iyi performans göstermiştir. Örneğin, %100 plastik gerinimde, 375 narinlik oranına sahip AL-5754 panel %48,9'a varan bir azalma gösterirken, aynı boyuttaki ST-37 panel yalnızca %33'lük bir azalma göstermiştir.

İncelenen paneller arasında, ST-37 malzemesinden üretilen, 2 mm kalınlığında ve 500 mm kenar uzunluğuna sahip panel, plastik gerinime karşı en düşük hassasiyeti göstermiş ve %2'den daha az bir kapasite kaybıyla neredeyse tam burkulma kapasitesini korumuştur. Buna karşılık, AL-5754 malzemesinden üretilen, 2 mm kalınlığında ve 750 mm kenar uzunluğuna sahip panel en yüksek hassasiyeti göstermiştir. Bu bulgular hem malzeme seçiminin hem de geometrik özelliklerin (incelik oranı ve kalınlık gibi) panelin ikincil burkulma yükü ve burkulma sonrası performansı üzerinde önemli bir etkiye sahip olduğunu ortaya koymuştur. Panellerin

plastik deformasyona uğrayıp yeniden yüklenebileceği yapısal uygulamalar için ST-37, burkulma sonrası yüksek stabilite ve yük taşıma kapasitesi gerektiren tasarımlar açısından daha güvenilir bir malzeme olarak öne çıkmıştır; özellikle daha kısa ve kalın konfigürasyonlarda. Bu da ST-37'yi, aşırı yükleme veya yeniden yükleme durumlarıyla karşılaşabilecek yapılar için uygun bir seçenek hâline getirmektedir.

Yapılan tüm bu çalışmaların ardından çalışmanın ana amacı, başlangıçtaki kritik burkulma yüklerini farklı plastik gerinim seviyeleri altında hesaplanan ikincil burkulma yükleriyle karşılaştırmak ve burkulma yükündeki azalma oranı ile panel boyutları arasındaki ilişkiyi ortaya koymaktır. Elde edilen bulgular, plastik deformasyona uğramış metal panellerin burkulma davranışının daha derinlemesine anlaşılmasına katkı sağlayacak ve mühendislik uygulamalarında yük taşıyan yapıların tasarımı ve güvenliği açısından önemli öngörüler sunacaktır.

1. INTRODUCTION

1.1 Motivation of the Thesis

The thin-walled structure is very common in engineering applications due to providing high strength to weight ratio, suitability for buckling driven design and ease of fabrication and assembly. In spite of advantageous of the thin-walled structure, there are some critical concerns to analyze them such as calculating and analyzing the critical buckling load and the associated buckling behavior, which can lead to sudden deformation.

To conduct linear buckling analysis, finite element method (FEM) is an approach that is commonly utilized. Eigenvalue equations are solved to calculate critical buckling load in the linear buckling analysis. Furthermore, the analytical formulations and empirical buckling constants are used.

In addition to initial buckling, analyzing post-buckling behavior beyond the initial buckling point is another critical concern to obtain optimized structural design. Hence, industries like aerospace, naval and structural industries that prioritize weight reduction focus on post-buckling analysis. While stress redistribution, the formation of new equilibrium paths, and the formation of secondary buckling events have been extensively studied, further research is still needed to determine how plastic deformation influences the critical buckling load of panels subjected to reloading.

Plastic deformations caused by overloads or in-plane loads during post-buckling stage can alter the mechanical response of panels, and can lead to a reduction in structural stiffness. This reduction can significantly decrease in the critical buckling load.

By conducting novel research that integrates both numerical simulations and experimental study, optimized designs that meet the demands of structural stability and integrity can be developed. These provide not only safety but also contribute to advancements in material efficiency and sustainability.

1.2 Aim of the Thesis

During the post-buckling stage, plastic deformation may occur due to the unexpected service loads, which alters the stiffness of thin-walled structures and affects their buckling resistance. However, the extent of this change and its impact on structural performance have not been thoroughly studied. The objective of the thesis is to investigate the effect of plastic strain developed during the post-buckling stage on the critical buckling load of panels under in-plane shear loading.

To achieve this objective, both experimental and numerical analyses are conducted. An AL-1050 alloy thin square panel with a side length of 330 mm and a thickness of 1 mm is utilized to perform experimental study. Furthermore, a picture frame test setup is employed to apply in-plane shear load. Totally, two strain gauges are placed on the panel to measure plastic and elastic strain.

For the numerical study, the finite element simulations are performed in Abaqus software to evaluate the impact of different level of plastic strains on the critical buckling load. The new calculated critical buckling load is named secondary buckling load in this thesis. These plastic strains are taken from the post-buckling stage at the ultimate buckling load, and used as predefined inputs in the simulations. Four levels of plastic strain such as 25%, 50%, 75%, and 100% are used to examine their effect on the panel's buckling performance.

A total of 18 different panels are modelled for the numerical analysis by using AL-5754 alloy and ST-37 materials. For each material, panels are modeled with 500 mm, 750 mm, and 1000 mm side lengths and 2 mm, 3 mm, and 4 mm thicknesses.

This research aims to compare the initial critical buckling load with the secondary buckling loads calculated for different level of plastic strains, and to identify a relationship between the reduction percentage and the panel's geometrical properties. The findings will contribute to a deeper understanding of post-buckling behavior in engineering structures and provide guidelines for design improvements and failure prevention in load-bearing applications.

1.3 Literature Review

The field of structural mechanics has been focused on the stability and integrity of structure under various loading conditions. The ability to understand and predict the buckling behavior of metals is crucial for ensuring the safe design of structures across numerous industries, including aerospace, civil engineering, and automotive engineering.

Research on panel buckling began in the early 1800s. In 1822, Navier calculated the stability equation for a rectangular panel based on Kirchhoff's theories [1] . Saint Venant extended on Navier's equation by including the effects of edge and shearing forces along the axial direction [2] . Later, Bryan derived the critical buckling stress equation for a rectangular panel with simply supported boundary condition under uniaxial compression to calculate the values the critical load values using the energy approach [2] .

Timoshenko proposed a novel solution for the same problem. He assumed that when a panel buckles, it takes the form of a sinusoidal half-wave in the compression direction [3] . In addition to simply supported panels, buckling of panels that are uniformly compressed and with two of edges perpendicular to the load direction simply supported, while other edges were subjected to various boundary conditions is explored by Timoshenko. The result can be found in standard texts [4] [5] . In addition to that, Lundquist and Stowell and Wang have solved the buckling problem of panel under in-plane shear using energy method. Lundquist and Stowell applied energy method to two edges elastically restrained and two edges simply supported panels, while Wang applied it to simply supported panels [6] .

The document is written by G. Gerard and H. Becker is published under auspices of the National Advisory Committee for Aeronautics (NACA). The document provides a comprehensive review of the available theories and test data on the buckling of curved panels and shells. It covers various load conditions such as axial compression, bending, torsion, and external pressure. The document focuses on both elastic and inelastic buckling behaviors, and the report discusses the discrepancies between linear theory and experimental data in several cases, particularly for curved panels and cylindrical shells [7] .

There are many studies about panels under combined loading. For example, Batdorf and Houbolt has studied to derive solution for infinitely long elastically restrained panel that are loaded shear and transverse direct stress load [8] . After that, the buckling problem of simply supported panels under combined shear and longitudinal direct stress is investigated by Batdorf and Stein. They used the energy approach to study panels with different length-width ratios [9] . Johnson and Buchert employed the energy method to investigate the buckling behavior of rectangular panels that are under combined load which are bending, shear, transverse compression. The panels are applied either simply supported or elastically restrained on compression edge, while the tension edge was simply supported as boundary condition [10] . Furthermore, Kang and Leissa presented exact solutions for the buckling load of rectangular panels. While the two opposite edges of panels have simply supported, the other two edges remain free [11] .

Y. Xiang et.al. studied about influence of internal hinge on elastic buckling of rectangular panels using Levy method. These panels loaded by biaxial or uniaxial loads have simple support boundary conditions that are applied on two opposite edges [12] . Later that, he published a novel paper to calculate buckling load of panels by determining buckling factors for different type of boundary conditions and aspect ratios is calculated using Ritz method [13] . The study written by Chen Yu is focused rectangular panel buckling problem. Elastic and plastic buckling of panels that have different aspect ratios, loading location and boundary conditions are investigated. Panels have simple supports on two opposite edges that are aligned to applied load and there are different combinations of boundary conditions on the other two edges like clamped, free or simple support for different panels [6] .

After the initial buckling event, understanding and predicting post-buckling behavior of the structure are essential for optimizing designs, ensuring safety, and extending the operational life of aerospace structures. The post-buckling response of metallic panels has been extensively studied due to its importance in thin-walled structures widely utilized in aerospace, civil, and mechanical engineering. Early studies, such as those by Alinia et al. and Amani et al., laid the groundwork by investigating the post-buckling responses of unstiffened panels made from materials like aluminum, stainless steel, and carbon steel. These studies focused on how slenderness ratios and initial imperfections effect load-bearing capacity and the overall stability of structures under

shear and axial loads [14] [15] . The influence of geometric imperfections on post-buckling behavior has been another critical area of research. Study of Ghadami and Broujerdian provided the formula to calculate reduction factor applied on post-buckling load. The reduction factor is used because of initial imperfection [16] . Elgaaly further contributed by developing computational models that accurately predict the post-buckling behavior of thin steel panels, accounting for both geometric and material nonlinearities, and demonstrating strong correlations with experimental results [17] .

The complexities associated with wrinkling and buckling phenomena in sheet metal forming have also been thoroughly studied. Cheng et al. developed a stress-based wrinkling predictor integrated with the LS-DYNA FEM package, providing significant advancements in both experimental and numerical methods for predicting post-buckling behavior. This study has significantly increased the accuracy and reliability of simulations used in design and analysis of structural components [18] . Similarly, Rasool and Singha employed finite element analysis to examine the nonlinear behavior of rectangular shear panels, highlighting how in-plane boundary conditions and out-of-plane restraints can affect stability and post-buckling performance [19] .

In addition to flat panels, another structural element that has received considerable attention is the curved panels. The research by Ljubinković et al. demonstrated that curvature and aspect ratio significantly affect the structural integrity of cylindrically curved steel panels under shear loads [20] . Furthermore, Amani et al. investigated the post-buckling behavior of curved panels under shear load, utilizing finite element analysis (FEA) to account for both geometrical and material nonlinearity. Their study examined panels with varying aspect ratios and curvature parameters to calculate elastic and post-buckling loads [21] . Additionally, Park and Seo further contributed to this field by developing an analytical method for simulating the post-buckling behavior of curved panels under axial load [22] . Besides that, Melcon and Ensrud have developed analytical methods for evaluating the buckling and post-buckling behavior of stiffened curved panels under combined loading [23] .

Apart from flat and curved plates, web girders and stiffened panels have been the subjects of extensive research due to their widespread use in structural engineering. Lee and Yoo carried out experimental studies on the ultimate shear strength of web

panels, challenging traditional tension field theories and revealing discrepancies between conventional failure mechanisms and actual shear behavior. Their work highlighted the importance of considering high bending stresses at failure, which are often neglected in conventional design approaches [24] . More recently, Xue et al. investigated the post-buckling shear capacity of high-strength steel plate girders, comparing results obtained from FEM simulations and EC3 formulas [25] , while Yuan et al. analyzed the shear resistance of aluminum alloy extruded H-Section beams, emphasizing the significant influence of end post rigidity and aspect ratio on shear capacity [26] [25] . Further advancing the understanding of shear resistance and local buckling behavior, Ibrahim et al. conducted a comprehensive experimental and numerical analysis for unstiffened web-tapered steel members to provide design procedure. Similarly, Wang et al. focused on aluminum I section beams, developing novel design methods tailored to the unique properties of aluminum alloys [27] .

Stiffened panels, which are commonly used in aerospace structures, have also been extensively studied. Cricrì et al. proposed new multi-hinged fixtures for testing stiffened and unstiffened aluminum panels under shear loads. Their experimental results were validated using numerical simulations generated with ANSYS, providing a reliable method for evaluating the post-buckling behavior of these panels [28] . Hussain and Loughlan further studied the buckling and post-buckling response of stiffened plates under combined shear and compression loads to demonstrate how stiffeners improve structural stability under complex loading conditions [29] . Furthermore, Featherston et al. investigated the post-buckling behavior of stiffened panels subjected to combined shear, compression, and in-plane bending loads. Their research revealed that redistribution of the into stiffeners after initial buckling has an important effect on the maintaining structural integrity and load bearing capacity of the panels [30] . Similar to these studies, research by Alinia and Shirazi focused on the design of stiffeners in steel plate shear walls, revealing that unidirectional stiffeners offer more effective buckling resistance compared to bidirectional configurations [31] . Prato et al. extended this research by investigating the effects of geometrical imperfections and joints on the buckling and post-buckling behavior of thin-walled stiffened panels. Furthermore, they compared experimental data obtained from plates made of aluminum alloy with attached L shape stiffeners [32] . Significance of the role of material properties in post-buckling behavior has also been studied. Guan et al.

investigated the post-buckling behavior of titanium alloy stiffened panels under shear load, examining the effects of stringer dimensions and panel thickness on buckling and post-buckling loads. Their findings contribute to the optimization of design parameters for titanium alloys, which are increasingly used in aerospace applications due to their high strength-to-weight ratio [33] .

Besides these studies, there are papers where post-buckling regime of plate is investigated with evaluating the elastic and plastic strains. Glassman and Garlock proposed the compression-based approach to predict the ultimate post-buckling shear strength of steel plates. In their approach, the role of diagonal compression is highlighted in shear buckling. Also, the approach is compared with approach developed by Basler [34] and validated with experimental results [35] . Alinia et al. studied on thin steel shear panels to investigate influence of geometric properties and boundary conditions on occurred yield zone and bending stresses while reaching post-buckling load [36] . Besides, Garlock et al. analyzed a plate which has 1.0 aspect ratio and 134 slenderness ratios to evaluate occurred stress such as membrane, principal stresses and their directions with validated FE model [37] . Wang et al. analyzed plates under pure shear load and various boundary conditions that represent stiffeners and flanges. The aim of study is finding the optimal boundary condition to represent plate girder and presenting comprehensive description for development of membrane stresses during post-buckling regime [38] .

1.4 Content of the Thesis

The organization of content of the thesis is designed to enhance clarity and comprehension. The report is organized as follows:

- Chapter 2. provides a theoretical background, analytical methods for linear buckling, and non-linear analysis approaches, including the Newton-Raphson and Modified Riks methods
- Chapter 3. presents the experimental study, detailing the test specimens, material properties, loading conditions, instrumentation, and testing procedures used to investigate the post-buckling behavior of panels subjected to shear loading.

- Chapter 4. describes the finite element model, outlining the methodology of the numerical analysis and the validation of the finite element results with both literature and experimental data.
- Chapter 5. discusses the results and findings, comparing the linear and post-buckling behaviors of different panels. Furthermore, the effect of plastic strains and geometrical properties on the secondary buckling load are evaluated.

2. THEORITICAL BACKROUND

2.1 Introduction

In the thesis, linear buckling analysis is conducted and post-buckling analysis are performed using non-linear analysis methods. In this section brief theoretical backround of methods of these analysis are presented.

2.2 Analytical Calculation of Linear Buckling

In the structural analysis, one of the significant failure modes is buckling of component. While various methodologies exist for calculating the buckling of bars, beams, shells, and panels, this thesis specifically focuses on the shear buckling behavior of flat panels. The theoretical approach of shear buckling of flat panel is outlined in this section.

The critical shear buckling stress of panel is calculated using (2.1). While E and ν represent elastic modulus and Poisson ratio of panel material respectively, t and L are related with geometric properties of panel.

$$F_{cr} = \frac{k_s * E * \pi^2}{12 * (1 - \nu^2)} * \left(\frac{t}{L}\right)^2 \qquad (2.1)$$

The k_s parameter in the equation represents buckling coefficient depends on panel edge boundary condition and aspect ratio of panel. For panel under shear loading and under clamped boundary condition, buckling coefficient can be found from graph in Figure 2.1 [39] . The graph is drawn aspect ratio vs buckling coefficient for clamped edges and hinged edges.

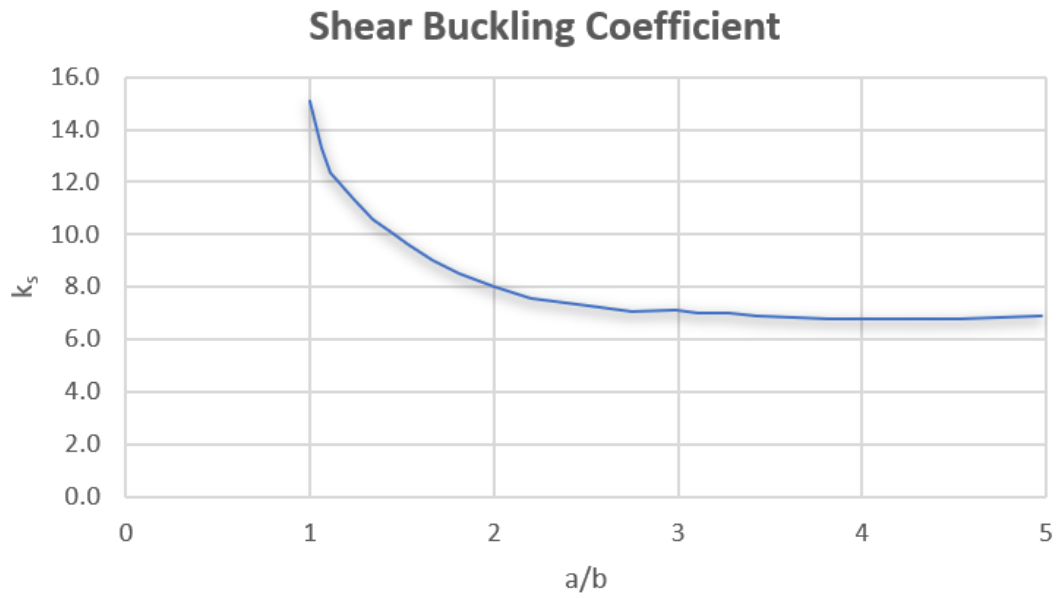

Figure 2.1 : Shear buckling coefficient of plates as a function of a/b for clamped and hinged edges [39] .

2.3 Non-Linear Analysis Methods

Nonlinear analysis in FEM involves studying systems where the relationships between variables are not linear. A series of linear solutions is calculated iteratively to approximate the nonlinear solution [40] . The analysis conducted in this thesis is non-linear analysis, which cannot be solved using direct analytical methods.

In the nonlinear analysis, the nodal force vector (r(u)) must be equal the applied load (f) vector in each state as shown in (2.2) [41] .

$$f^t - r^t = 0 \qquad (2.2)$$

The state and interval are described using t and Δt, respectively in (2.2). If the (2.2) is provided, the equilibrium of next step has to be provided like (2.3).

$$f^{t+\Delta t} - r^{t+\Delta t} = 0 \qquad (2.3)$$

Also, nodal force can be written like (2.4) in which (Δr) represents nodal force change due to change of displacement (Δu). To obtain tangent stiffness matrix like in (2.6), r(u) is expanded with first order Taylor expansion like in (2.5).

$$r^{t+\Delta t} = r^t + \Delta r \tag{2.4}$$

$$r(u) \approx r(u^t) + \frac{\partial r}{\partial u}|_{u^t} * (u - u^t) \tag{2.5}$$

$$K^t = \frac{\partial r}{\partial u}|_{u^t} \tag{2.6}$$

With combining (2.5) and (2.6), the change of nodal point force is obtained approximately in (2.7). Then, the change of displacement is formulated by substituting (2.4) and (2.5) into (2.3).

$$\Delta r = K^t * \Delta u \tag{2.7}$$

$$K^t * \Delta u = f^{t+\Delta t} - r^t \tag{2.8}$$

Also, the displacement is obtained like (2.9). Owing to (2.5), the obtained equation for displacement gives result approximately.

$$u^{t+\Delta t} = u^t + \Delta u \tag{2.9}$$

This situation necessitates iterative numerical methods to solve equations. The common used numerical methods that can solve the equations iteratively are load control method (LCM), displacement control method (DCM), Newton-Raphson method, Modified Newton-Raphson method, arc length method.

While the numerical methods except arc length method can be used for the cases where the structure's response is not constrained by the limit point, the arc length method is used to solve when interesting the structure response of beyond limit point [42] [44] . Below, the Newton-Raphson method and arc length method are explained.

2.3.1 Newton – Raphson Method

In nonlinear structural analysis, the Newton-Raphson method is extensively employed to solve equilibrium equations iteratively. The total load is applied in multiple step starting from zero and gradually increasing to the desired level. While incrementation does not have to be equal for each iteration, difference between external nodal forces and internal nodal forces have to be eliminated or lower than desired tolerance to achieve convergence [45] .

One of the key features of the Newton-Raphson method is that the tangent stiffness (K_t) updated in every iteration. While the specification brings high accuracy and robust

convergence, it creates high computational costs, especially for complex models. To reduce computational cost of Newton-Raphson method, the modified Newton-Raphson method is developed. In this method, internal nodal forces are updated in every iteration, while tangent stiffness matrix is recalculated only at the start of each load step [46] [47] .

Although the modified method may result in slower convergence compared to the classic approach, it offers a practical trade-off between accuracy and efficiency, making it suitable for many engineering applications.

2.3.2 Modified Riks (Arc Length) Method

Even though the Newton-Raphson method is commonly used for nonlinear solution, it faces significant challenges in snap-through problems and configurations involving sudden changes due to the Newton-Raphson method relies on a continuous and monotonic load-displacement path.

The relationship between load and displacement, along with its critical points, is graphically illustrated Figure 2.2. A and D points are referred as load limit point which represent significant deformation is occurred in case of sustaining additional load. Besides, displacement limit points (B and C) indicate points having equilibrium solution and very sensitive to displacement changes.

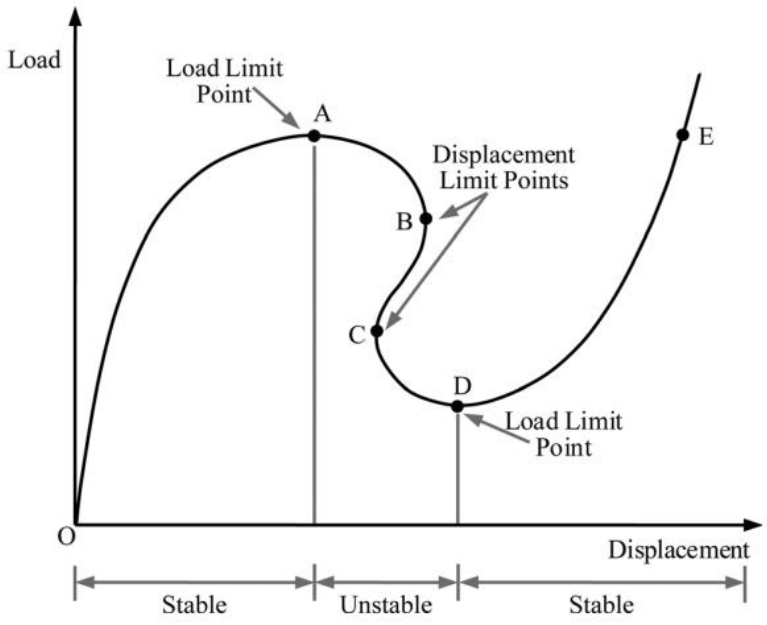

Figure 2.2 : Non-linear equilibrium paths [48] .

Due to instability of system between load limit points, it is required to change both load factor and displacement to solve equations. Because the unknown parameter is increased, additional equation should be solved to resolve problem of under-determined system of equations. The additional equation named the arc-length equation is given in (2.10) [42] .

$$[\Delta u]^T * [\Delta u] + \Psi * [\Delta \lambda]^2 * f^T * f = [\Delta s]^2 \qquad (2.10)$$

ψ parameter in the equation represents arc-length scheme parameter which depends on arc-length method. Besides, s called as arc-length parameter is used to parametrize the equilibrium path. The graphical demonstration of arc-length method can be seen from Figure 2.3.

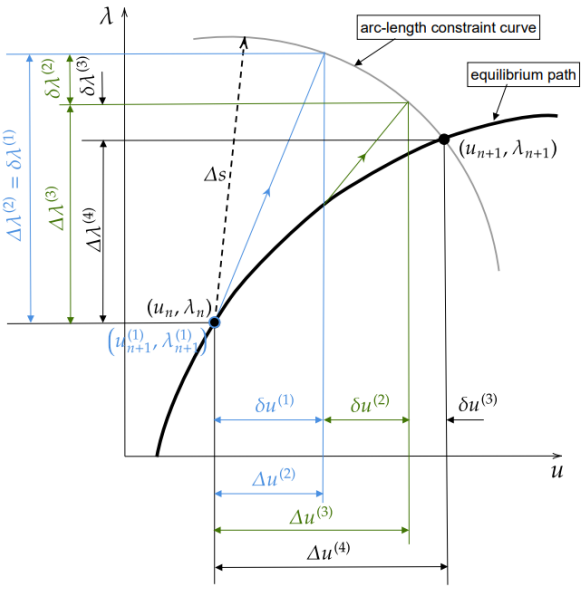

Figure 2.3 : Iteration of arc-length method [42] .

3. EXPERIMENTAL STUDY

3.1 Introduction

It is essential to understand the buckling behavior of panels for the applications in structural and aeronautical engineering. The aim of the conducted experimental study is to investigate the behavior of metallic panels that have undergone plastic deformation under shear loading and to validate the results obtained from numerical study in the thesis. The following sections give detailed information about test specimen, setup, instrumentation, and methodology.

3.2 Test Specimen and Material Properties

The experimental study focused on a thin square metallic panel is made from Aluminum 1050 alloy, with dimensions of 330 mm × 330 mm and a thickness of 1 mm. The dimensions of the panel were determined based on FEM validation findings from the literature, as detailed in Section 4.3.1 .

The material was assumed to be isotropic and homogeneous and its mechanical properties are presented in Figure 3.1 taken from [43] . The aluminum alloy used in this study has a Young's modulus of 68 GPa, a yield strength of 50 MPa, and a Poisson's ratio of 0.33.

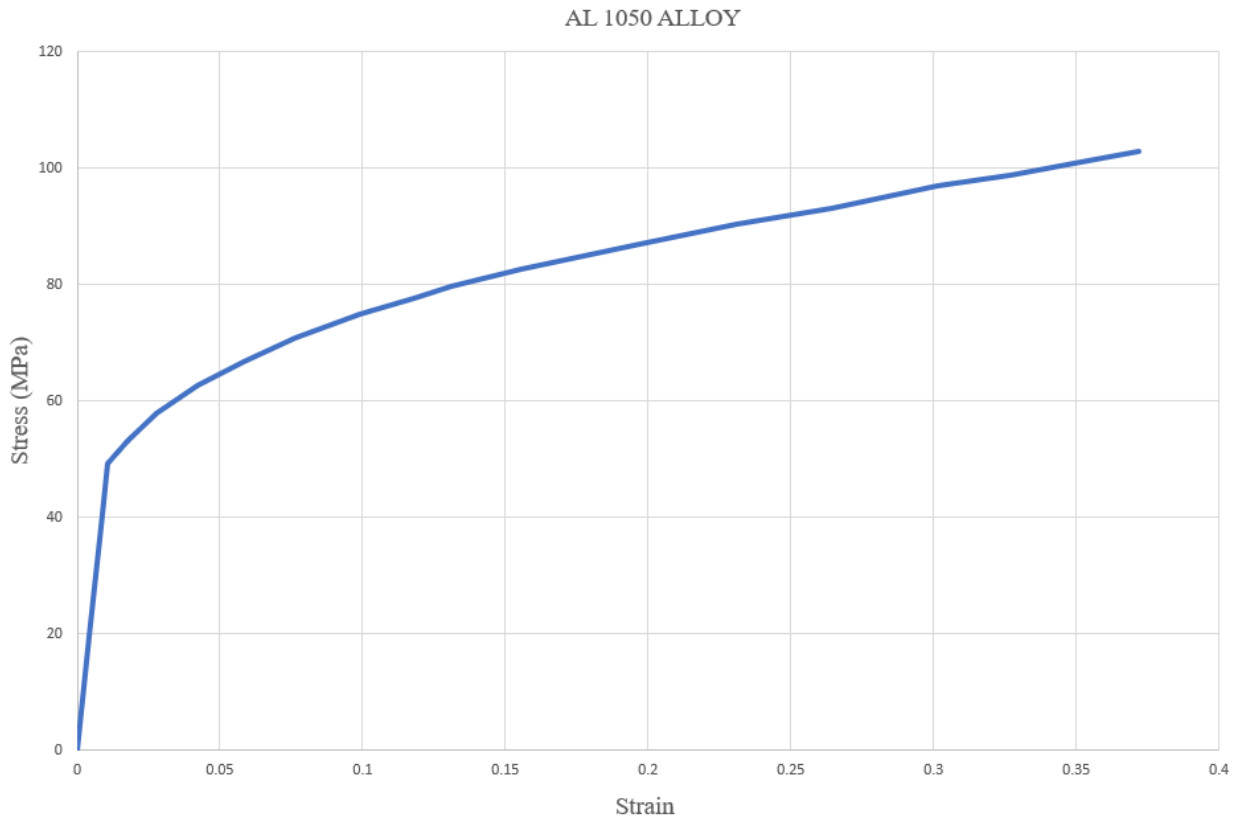

Figure 3.1 : The stress-strain curve of AL-1050 alloy [43] .

3.3 Loading and Test Setup

To perform the experimental study, a custom designed picture frame test fixture was designed. The test fixture enables to apply in-plane shear loading with ensuring precise force application and controlled deformation mechanism. The test fixture was integrated with a Shimadzu AG-IS universal testing machine having a capacity of 600 mm stroke and 50 kN.

The picture frame test fixture consists of eight rigid rectangular aluminum bars, each with dimensions of 5 mm × 25 mm. The test specimen an aluminum panel was fastened to the edge of square panel. A total of 20 fasteners per edge were assembled with 4 mm fasteners to ensure a uniform clamping boundary condition and to prevent slippage during loading as shown in Figure 3.2. The panel was clamped between these frame sections, with two bolted lines along each edge to establish a clamped boundary condition and ensuring a well-defined load transfer.

At each corner of the square panel, 8 mm diameter bolts were installed to provide hinge points. They allow relative rotational movement of the bars, which is a critical aspect for generating pure shear deformation.

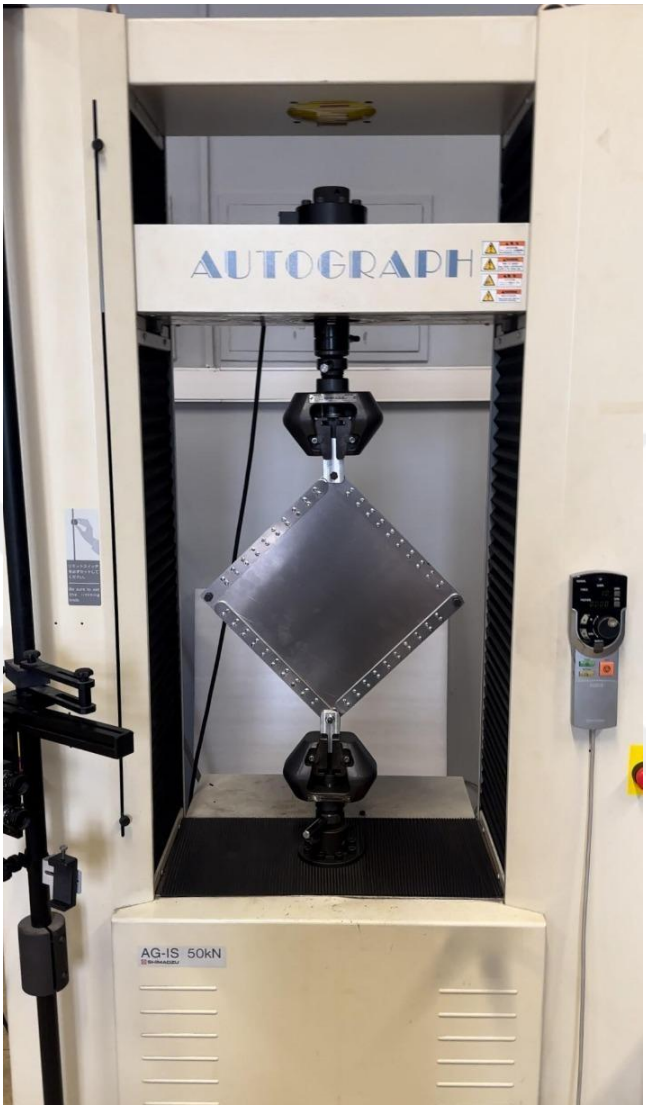

Figure 3.2 : Picture frame test fixture.

To transmit the tensile load from the test machine to the fixture, Y-shaped connector components machined from 6061 aluminum alloy were employed. These connectors are designed to align the load diagonally through the hinged corners of the frame, ensuring symmetric and uniform shear deformation of the panel.

3.4 Instrumentation and Measurement

To capture strain distribution and deformation characteristics, strain gauges were mounted on both sides of the plate. Each strain gauge was positioned such that its

center is located 95 mm away from the edges of the panel, ensuring measurement accuracy at a critical region susceptible to shear and post-buckling effects.

The used strain gauge type is KFGS-5-120-D17-11 (L3M3S) which capable of recording principal strain components in multiple directions with 3 axis-rosette strain gauge.

The strain data was collected continuously during the test using the Dewesoft HS-STGS data acquisition (DAQ) system that provides high-resolution and synchronized strain measurements. This setup allows for a comprehensive evaluation of the panel's behavior under in-plane shear loading.

The results obtained from the experimental measurements were compared with numerical simulations to validate the finite element model. This comparison ensures the accuracy and reliability of the computational approach and supports the overall integrity of the study.

4. FINITE ELEMENT MODEL

4.1 Introduction

This section presents the finite element model employed for post-buckling analyses in this thesis. The selected settings such as element types, analysis methods and boundary conditions are explained in detail. Furthermore, the validations conducted using literature studies and experimental results to ensure the accuracy and reliability of the proposed FE model are described.

4.2 Methodology of Study

The finite element analyses were conducted via software ABAQUS to simulate panels under shear load. To create FE models, S4R elements which are shell element with reduced integration were utilized. The used shell elements have 5 integration points. In ABAQUS, nodes of S4R elements have 6 DOF with three rotational and three translational. Also, the 30x30 mesh was selected as minimum required mesh after mesh convergence study which can be found Section 4.2.1 detail.

In the Figure 4.1, the used boundary condition that provides clamped edges and pure shear loading is given. It can be seen that the edges of the plates can move freely in both directions. In order to compare and validate the numerical findings with the data that is theoretically accessible, the clamped boundary condition was used.

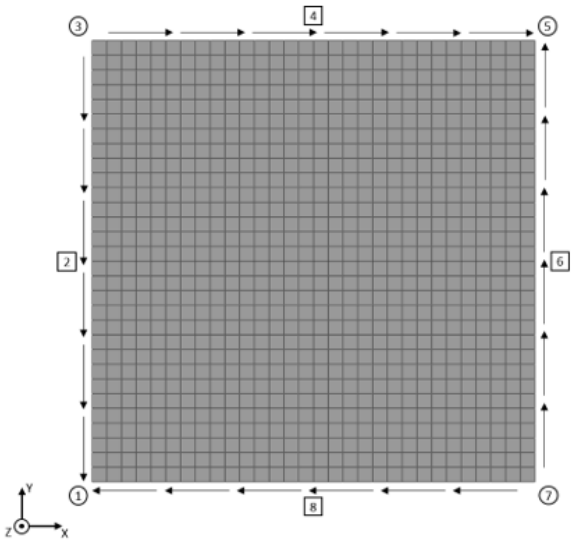

No	u_x	u_y	u_z	θ_x	θ_y	θ_z
1	■	■	■	■	■	■
2	□	□	■	□	■	□
3	□	□	■	■	■	■
4	□	□	■	■	□	□
5	□	□	■	■	■	■
6	□	□	■	□	■	□
7	□	□	■	■	■	■
8	□	□	■	■	□	□

□: Free ■: Fixed

Figure 4.1 : Boundary condition of FE model.

There are 3 different types of materials used in this thesis. The data were used to define materials were taken from stress-strain graphs found from literature. The stress-strain curve of AL-1050 alloy material which was used in experimental study given in Figure 3.1. Also, the stress-strain curve of ST-37 and AL-5754 alloy materials are given in Figure 4.2 and Figure 4.3, respectively.

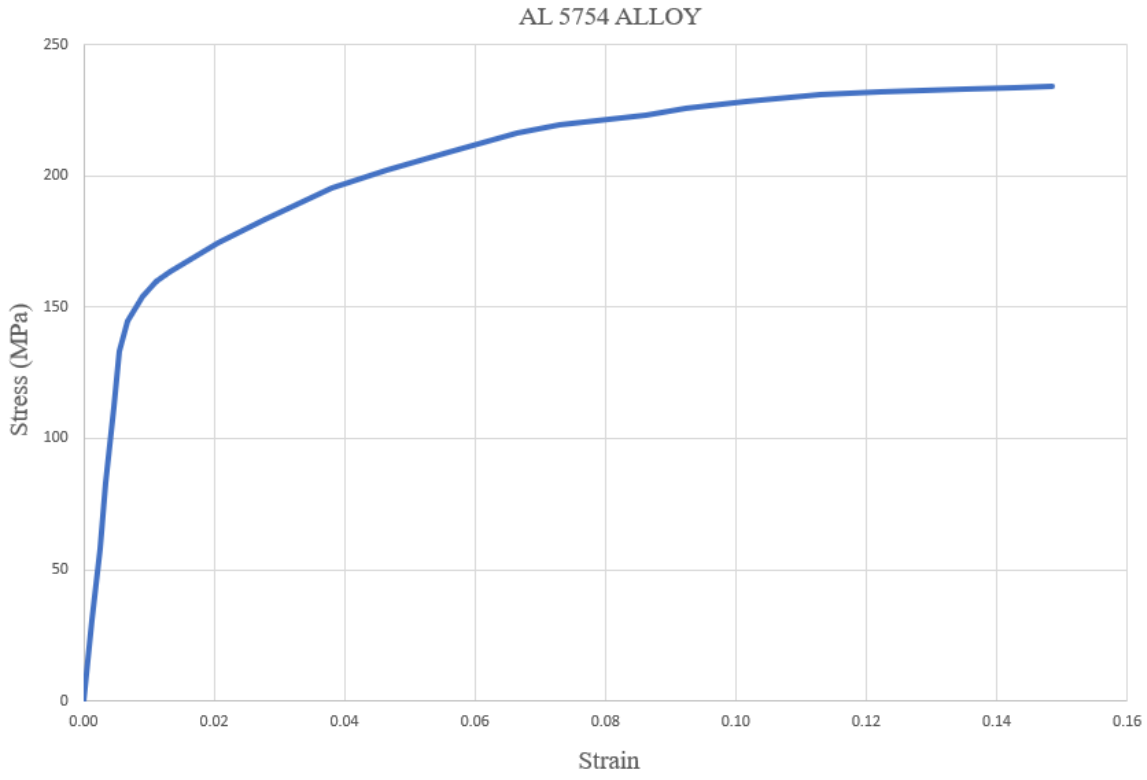

Figure 4.2 : The stress-strain curve of AL-5754 alloy [49] .

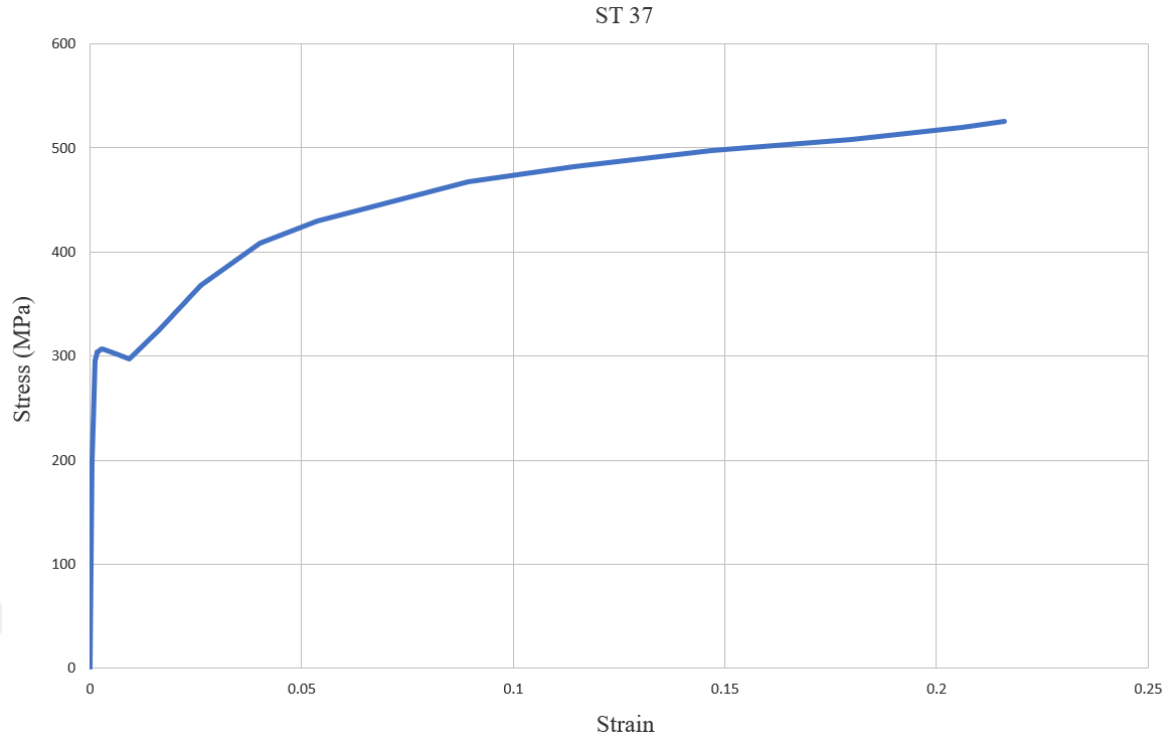

Figure 4.3 : The stress-strain curve of ST-37 [50] .

The FEM process consists of five steps designed to calculate the critical buckling load, the ultimate buckling load, and the secondary buckling load of the panel, as depicted below:

- The Linear Buckling Analysis (Eigenvalue Extraction)

  First, the eigenvalues and eigenmodes of the panel were calculated using a linear buckling analysis step, which employs the Lanczos eigen solver.

- The Nonlinear Post-Buckling Analysis (Static Riks Method)

  After obtaining the eigenmodes, the panel was analyzed using a Static Riks analysis step to determine its post-buckling capacity. Before conducting this step, the first eigenmode of the panel, shown in Figure 4.4, was introduced as an initial imperfection using the *IMPERFECTION command. The imperfection magnitude is set to t/100, where t is the panel thickness.

  The introduction of an initial imperfection is essential for this type of analysis, as it enables the structure's post-buckling behavior to be captured, allowing the ultimate load (F_u) to be determined. Without an imperfection, the model may not progress beyond the buckling bifurcation point, preventing an accurate post-buckling load-displacement response from being obtained [37] .

- Defining Plastic Strain After Post-Buckling

  To evaluate the secondary buckling load of the panel, the different levels of total strain such as 25%, 50%, 75%, and 100% developed in the post-buckling stage were separately transferred to new models using the *PREDEFINED FIELD function. The element middle of the panel is taken as reference element to determine different level of strains. This ensures that the residual plastic strains and deformations from the previous post-buckling analysis are correctly applied as the initial state in the new analysis.

- Strain Relaxation Step

  Since both elastic and plastic strain are developed while reaching the ultimate load, an additional static step was introduced to allow the elastic stain to relax, leaving only the plastic strain in the model. This step was created using same boundary condition, but external load was not applied.

- Secondary Buckling Load Calculation

  After completing the strain relaxation step, a linear buckling analysis was conducted with different level of the plastic strain to determine its secondary buckling load.

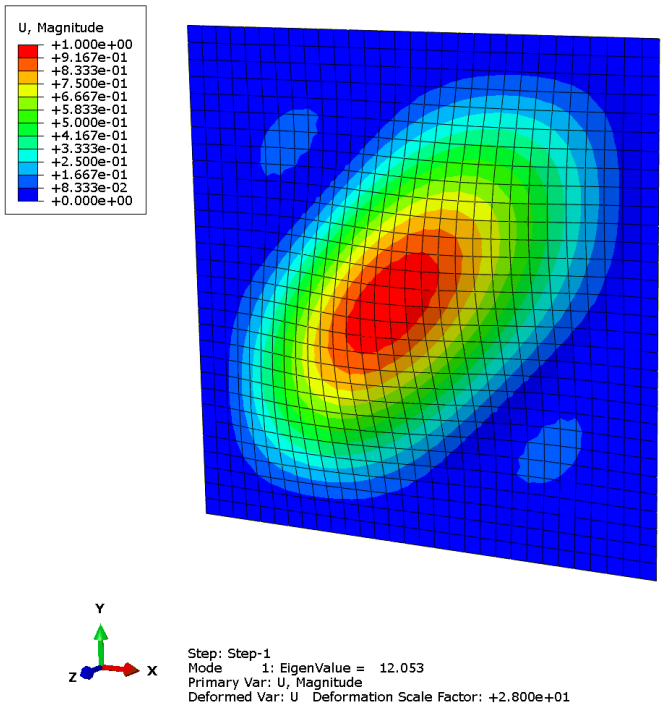

Figure 4.4 : First eigenmode of panel.

4.2.1 Mesh convergence study

A mesh convergence study was carried out in order to ensure the precision and reliability of the conducted FE analyses. Also, finding the lowest mesh density necessary to maintain computational efficiency while obtaining stable results for the critical buckling load is the aim of this study. Mesh convergence study was conducted with eigenvalue analysis by evaluating the lowest eigenvalue.

The critical buckling load of plates was calculated using the FE method for 10 different mesh densities, and the percentage error was determined relative to the theoretical buckling load. For this study, dimension of the used aluminum plate is 1000x1000x5 mm, the shear buckling coefficient was determined as 15 for given dimension from Figure 2.1 for clamped boundary condition. The critical buckling load was calculated as 63.466 kN using (2.1).

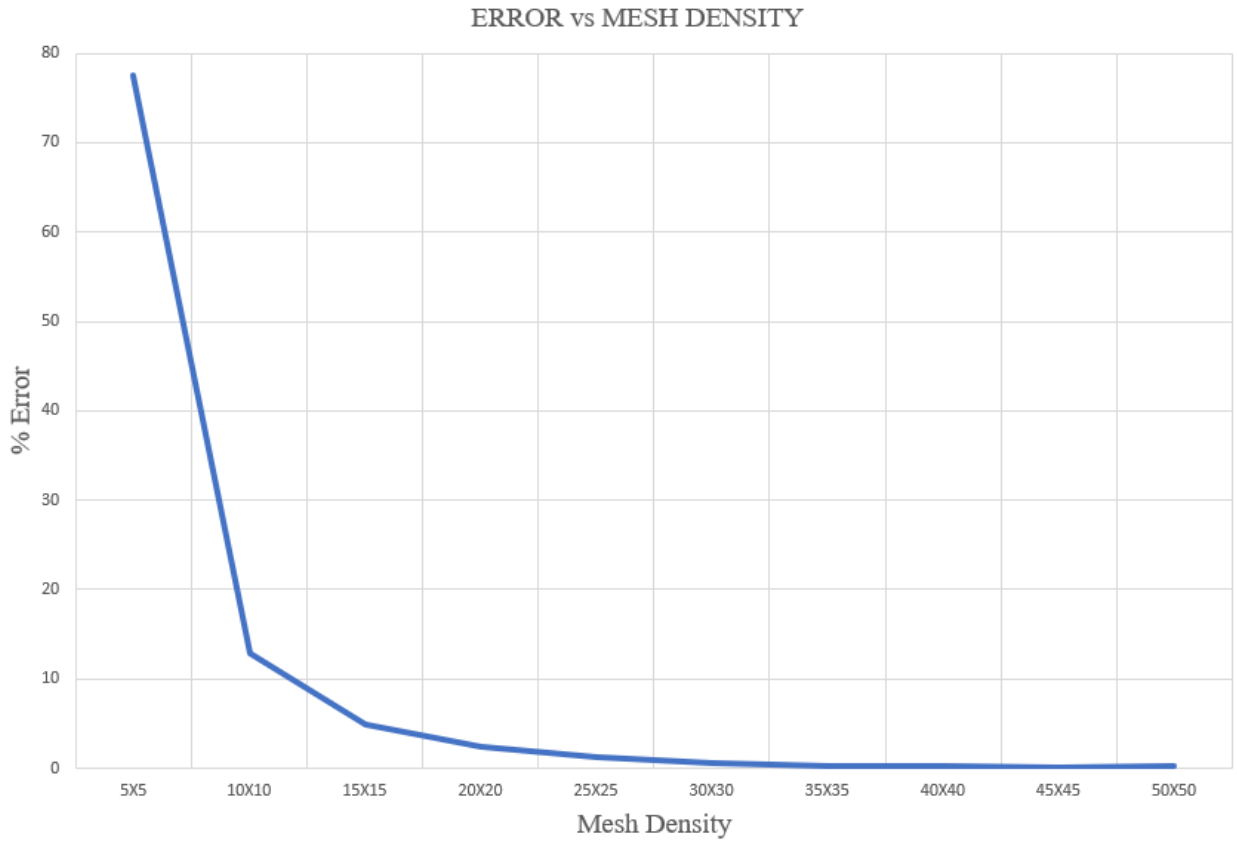

Figure 4.5 : Error vs mesh density graph.

The calculated error vs element number graph can be found from Figure 4.5. It can be seen that the error was calculated below 1% for finer than 30x30 mesh density. The 30×30 mesh density is selected for the final analysis based on the convergence results.

When compared to finer mesh density, this mesh density offered a balance between accuracy and computational cost with negligible differences in results. In addition to that the calculated critical buckling loads and the corresponding number of elements are given in Table 4.1. As can be seen from the table, as the number of elements increases, the critical buckling load converges to approximately 62.5 N an associated error of about 0.6%.

Table 4.1 : Error and critical buckling load of convergence study.

Number of Element	Critical Buckling Load (N)	Error (%)
25	110.90	77.5
100	70.50	12.9
225	65.55	4.9
400	63.95	2.4
625	63.25	1.2
900	62.85	0.6
1225	62.60	0.2
1600	62.50	0.02
2025	62.35	0.2
2500	62.30	0.3

4.3 Validation Finite Element Method

The main objective of this study is to determine the critical buckling load of panels that retain plastic strain after the post-buckling regime. To calculate this, the finite element model (FEM) consists of 3 steps was built. First, the linear buckling analysis was performed. Then, a post-buckling analysis was conducted using static Riks method as explained in Section 4.2. For these two steps, the finite element (FE) model was validated against the results from literature. The determination of the specimen dimensions and prediction of experimental results were made possible by the FE model, which has been validated using data from the literature.

In the final step, linear buckling analysis was conducted for the plate in its post-buckled state. To validate this step, an experimental study was carried out, as explained

in detail in Section 3. . With this experimental study, the secondary buckling load of panel and their strain values were validated.

4.3.1 Validation of finite element model with literature study

To validate first two steps of the finite element model, the calculated results were compared with those available in the study [10] . The key parameters, including boundary conditions, material, properties, and loading conditions, were carefully matched to ensure consistency. To complete the validation study from the literature, four different plates with the same width and length but different slenderness ratio (β) were analyzed. While selected width (W) and length (L) are 1000 mm, the slenderness ratios, which are the ratio of width and thickness (t), was chosen as 150, 140, 130, 120. In the study, the aluminum that has 503.2 MPa yield stress (σ_Y) was used as the material and the nonlinear stress-strain curve given in the study was defined to model its elastic and plastic behavior.

The comparison for the selected plates can be found in Table 4.2. The maximum difference was calculated as 1.99% for a slenderness ratio of 120. The results obtained from finite element analysis (FEA) and those from literature are 1098.44 kN and 1077 kN respectively. Hence, the maximum error was calculated to be less than %2. It can be concluded that created FE model for determining specimen dimensions and preparing experimental predictions provides reliable results.

Table 4.2 : Results and error of validation study.

Plate Name	W (mm)	L (mm)	t (mm)	β	F_U^{LIT} (kN)	F_U^{FEM} (kN)	$Error_{PB}$
AL-1000x1000x6.67	1000	1000	6.67	150	708.0	721.65	%1.93
AL-1000x1000x7.14	1000	1000	7.14	140	804.0	817.16	%1.64
AL-1000x1000x7.69	1000	1000	7.69	130	924.0	940.36	%1.77
AL-1000x1000x8.33	1000	1000	8.33	120	1077.0	1098.44	%1.99

4.3.2 Validation of finite element model with experimental study

The finite element model developed in this thesis was validated by comparing the numerical results with the experimental results to ensure its accuracy and reliability. For the validation, the key parameters including strain data and the ultimate buckling

load of the panel were evaluated. To obtain the experimental results, the three-axis rosette strain gauges were used as measurement instruments.

A strain threshold of 200 με (microstrain) was applied as a lower limit for data inclusion in the analysis. This cutoff was selected to exclude extremely small strain values that are typically within the measurement uncertainty range of the strain gauge system and may be influenced by background noise or minor surface irregularities. Strain values below this level are often not reliable for structural interpretation, particularly in the context of post-buckling deformation where meaningful strain localization is expected. By omitting data below 200 με, the analysis focuses on significant deformation behavior while ensuring a more accurate comparison between experimental and numerical results.

The experimental study was carried out in three stages. In the first stage, the panel was loaded beyond the critical point to reach the post-buckling regime and induce plastic strain. During this stage, the strain data correlation and the ultimate buckling load obtained from the experimental results were compared with the numerical results to verify the consistency of the data obtained from two methods.

The XY, XX and YY strain components up to the post-buckling stage are compared in Figure 4.6, Figure 4.7 and Figure 4.8 , respectively. These figures show that between experimental and numerical results exhibit strong agreement for all three strain components. In the numerical study, the ultimate buckling load and the XY strain data at the post-buckling were calculated as 5416.9 N and 659.04 με, respectively. The calculated strain is 624.9 με when 5294.6 N applied.

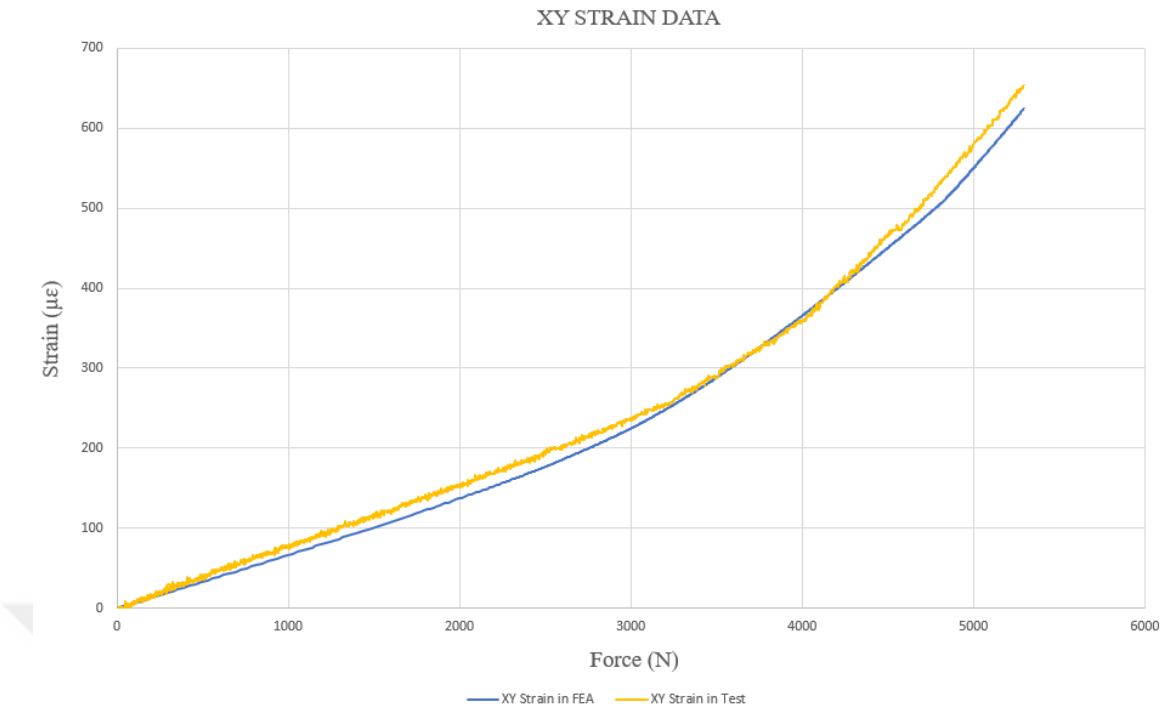

Figure 4.6 : XY strain data of experimental and numerical study for the first step.

In comparison, the experimental study yielded an ultimate buckling load of 5294.6 N and an XY strain of 653.4 με. The corresponding errors were calculated as 2.3% for the ultimate buckling load and 4.3% for the XY strain. The strain results for the other components and their calculated errors are summarized in Table 4.3

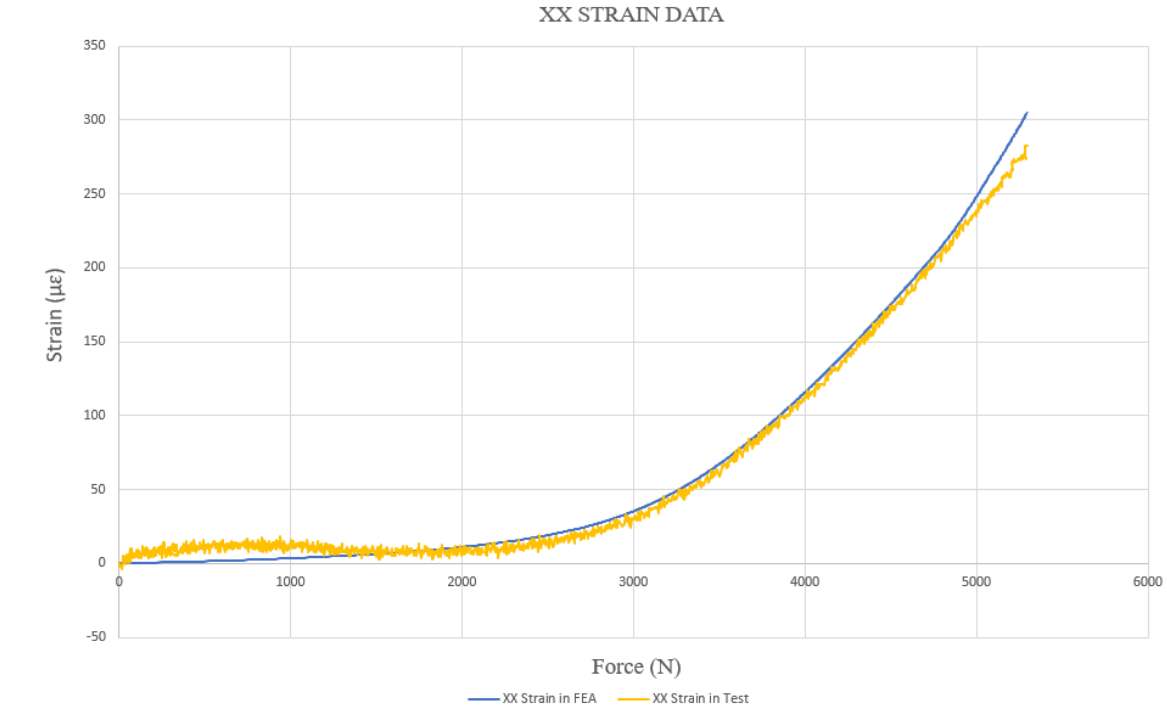

Figure 4.7 : XX strain data of experimental and numerical study for the first step.

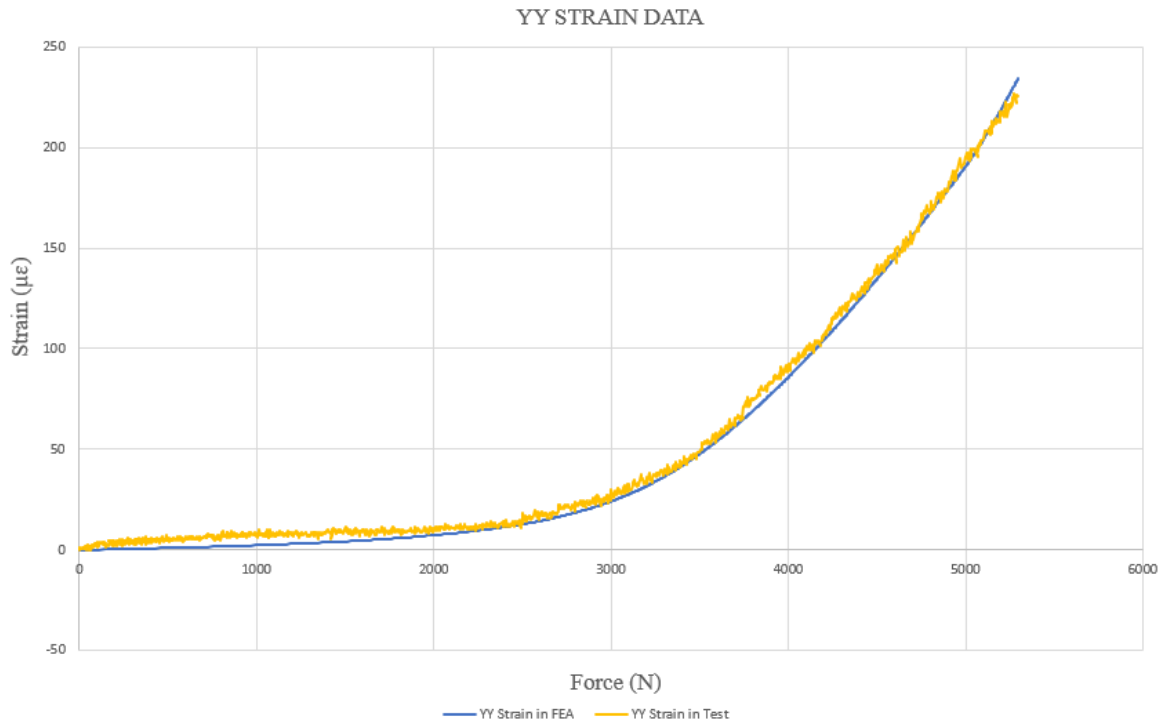

Figure 4.8 : YY strain data of experimental and numerical study for the first step.

In the second stage, the panel was unloaded, and the residual plastic strain remaining on the panel was measured.

In the final stage, the panel was reloaded to validate the strain response for a panel that had previously undergone plastic deformation. This reloading phase confirmed the FEM's ability to accurately capture the behavior of plastically strained panels under shear loading.

Table 4.3 : Strain result and calculated error.

Direction	$\mu\varepsilon_{EXP}$	$\mu\varepsilon_{NUM}$	Error %
XX	284.7	301.8	6.0
YY	225.3	234.2	4.0
XY	653.4	624.9	4.3

Additional strain data up to 4000 N are presented in Figure 4.9. The strain calculated from the FEA at this load level was 379.4 με, while the experimental value was 354.6 με. The close match between these values further demonstrates the accuracy and reliability of the developed finite element model.

Overall, the comparison between the finite element and experimental results demonstrated strong correlation across all evaluated parameters. The maximum deviation in strain values was 6.0% (in the XX direction), while the XY strain which is the most critical component under shear loading showed an error of only 4.3%. Similarly, the ultimate buckling load differed by just 2.3% between the experimental and numerical studies. These results indicate that the developed FE model is not only capable of capturing the general deformation trends but also provides high quantitative accuracy, validating its use for further simulations involving different materials and geometries.

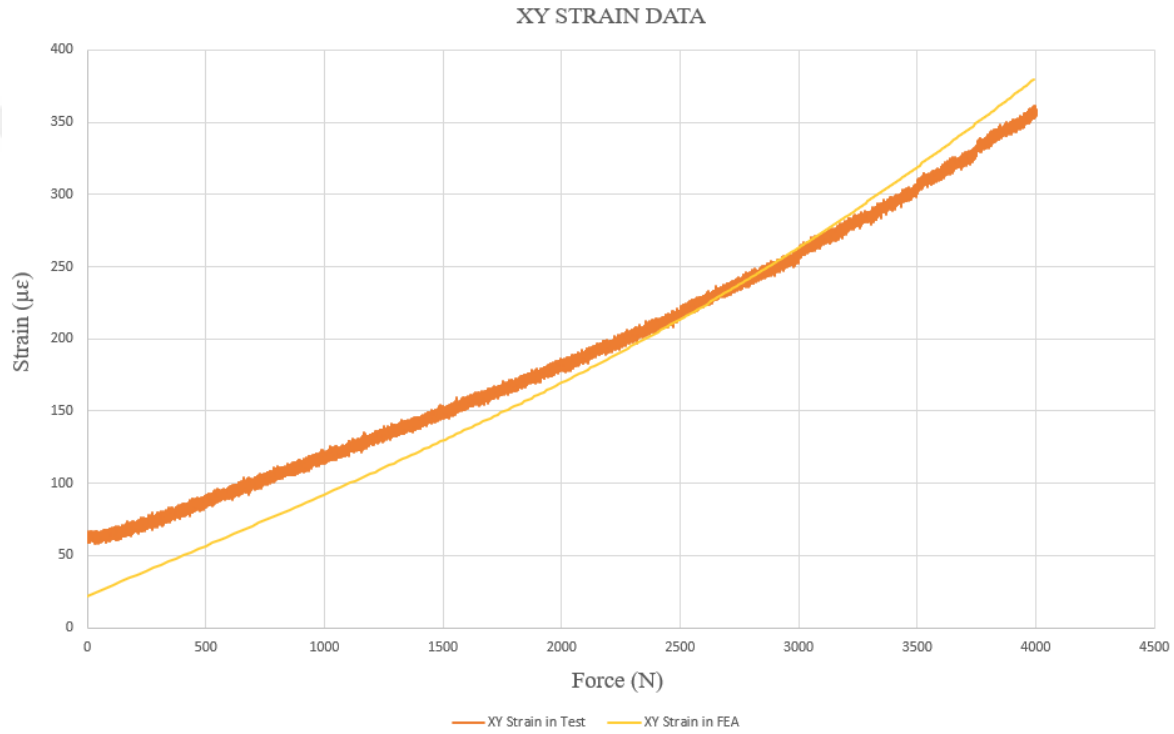

Figure 4.9 : XY strain data of experimental and numerical study for the reloading.

5. RESULT AND DISCUSSION

5.1 Introduction

In this section, the panels with different panel sizes, thicknesses and materials are investigated with regard to their buckling, post-buckling behavior and buckling behavior of plastically strained. The panels are modeled with square shapes. The selected side lengths are 500 mm, 650 mm, and 750 mm, and the thicknesses are 2 mm, 3 mm, and 4 mm for each size. These values are chosen to see how plastic strain affects the buckling and post-buckling behavior, and how this behavior changes with varying slenderness ratios.

Three different materials are used in the numerical study: AL-5754 alloy and ST-37. Each material has different mechanical properties such as Young's modulus and yield strength, which affect the buckling resistance of the panels. The material properties used in the analysis are given in Table 5.1.

Table 5.1 : Properties of the materials.

Materials	E (GPa)	σ_Y (MPa)	σ_U (MPa)	υ	Elongation (%)
AL-5754 Alloy	69.0	150.0	240.0	0.33	15.0
ST-37	210.0	300.0	530.0	0.30	22.0

In total, 18 panel models are created and analyzed. These models are used in all steps including linear buckling, post-buckling and secondary buckling.

The results of the linear buckling analysis are presented in the next section.

5.2 Linear Buckling Result

In this section, the results of the linear buckling analysis of the panels are presented for different sizes and materials. The Lanczos method was used as an eigen solver in Abaqus to calculate the critical buckling load (F_{CR}) and the corresponding mode shapes.

The critical buckling loads calculated with FE analysis and Eq (2.1) for each panel are listed in Table 5.2 and Table 5.3. As shown in the table, increasing the panel thickness or changing the material to one with a higher elastic modulus causes the critical buckling load to increase. This is expected because a stiffer panel resists buckling more effectively. Similarly, panels with larger side lengths show lower buckling loads due to their higher slenderness ratio.

Table 5.2 : The critical buckling loads of AL-5754 alloy panels.

Materials	F_{CR}^{FEM} (N)	F_{CR}^{Theory} (N)	Error (%)
AL57-500x500x2	15117.5	15269.05	0.99
AL57-500x500x3	50980.0	51533.03	1.07
AL57-500x500x4	120695.0	122152.4	1.11
AL57-650x650x2	11631.75	11745.4	0.96
AL57-650x650x3	39238.55	39640.8	1.01
AL57-650x650x4	92943.5	93963.4	1.08
AL57-750x750x2	10082.25	10179.4	0.95
AL57-750x750x3	34014.0	34355.4	0.99
AL57-750x750x4	80587.5	81343.9	0.92

The first buckling mode shape for selected panels is shown in Figure 4.4. The first mode is usually a shear-type deformation, where the panel buckles diagonally. This mode was used as an initial imperfection in the following post-buckling analysis.

The calculated maximum difference between result of FE analysis and theoretical study is 1.11%. These results show that the linear buckling analysis is valid, and the calculated mode shapes and loads can be used safely for the next steps of the post-buckling and reloading analyses.

Table 5.3 : The critical buckling loads of ST-37 panels.

Materials	F_{CR}^{FEM} (N)	F_{CR}^{Theory} (N)	Error (%)
ST37-500x500x2	45056.0	45505.8	0.99
ST37-500x500x3	151940.0	153582.3	1.08
ST37-500x500x4	359745.0	364046.8	1.20
ST37-650x650x2	34667.8	35004.5	0.97
ST37-650x650x3	116948.0	118140.2	1.02
ST37-650x650x4	277017.0	280036.0	1.09
ST37-750x750x2	30048.0	30337.3	0.96
ST37-750x750x3	101377.5	102388.2	1.00
ST37-750x750x4	240172.5	242697.8	1.05

5.3 Post-Buckling Result

In this section, the post-buckling behavior of the panels is investigated with using the nonlinear static Riks method to capture the load–displacement path until the ultimate buckling load (F_U) is reached. As mentioned before, the initial imperfection was defined using the first mode shape obtained from the linear buckling analysis at the beginning of the post-buckling analysis.

The XY strain vs. applied force curves for both sides of the AL57-750×750×3 panel are shown in Figure 5.1. As seen in the Figure 5.1, after the critical buckling load (34014.0 N), the strain curves start to separate because the panel goes into the post-buckling stage. In this situation, the panel continues to carry more load while the out of plane deformation increases. As the load increases, the panel stiffness decreases until the ultimate buckling load is reached. This point, where the strain curves suddenly rise in opposite directions, is called the ultimate buckling load (77900.9 N), and after that, the structure starts to soften.

The post-buckling stress distribution is also observed in the model. The stress becomes concentrated in the center area of the panel diagonally, which is consistent with the

expected shear deformation mode. The shape of deformation at the post-buckling stage is similar to the first mode shape, but the displacement is larger and nonlinear behavior is visible. The development of the stress until the ultimate buckling load is depicted in Figure 5.2 and Figure 5.3.

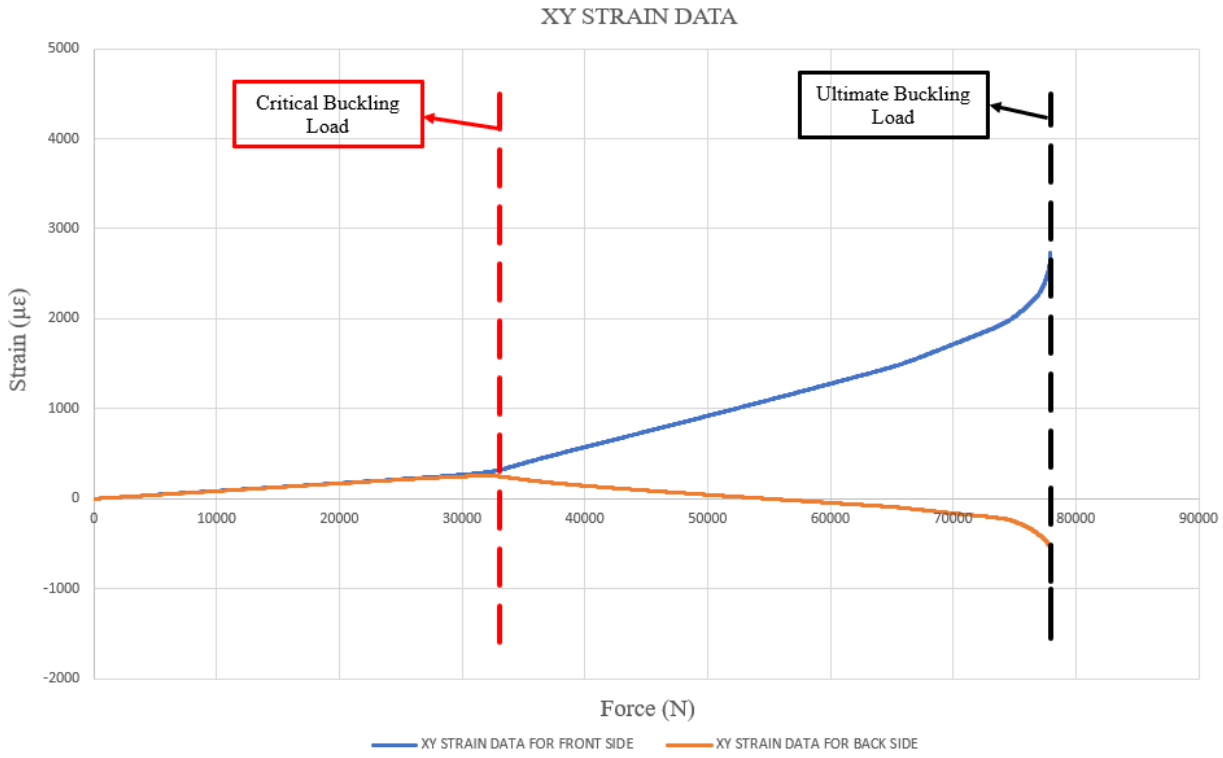

Figure 5.1 : XY strain data of AL57-750X750X3.

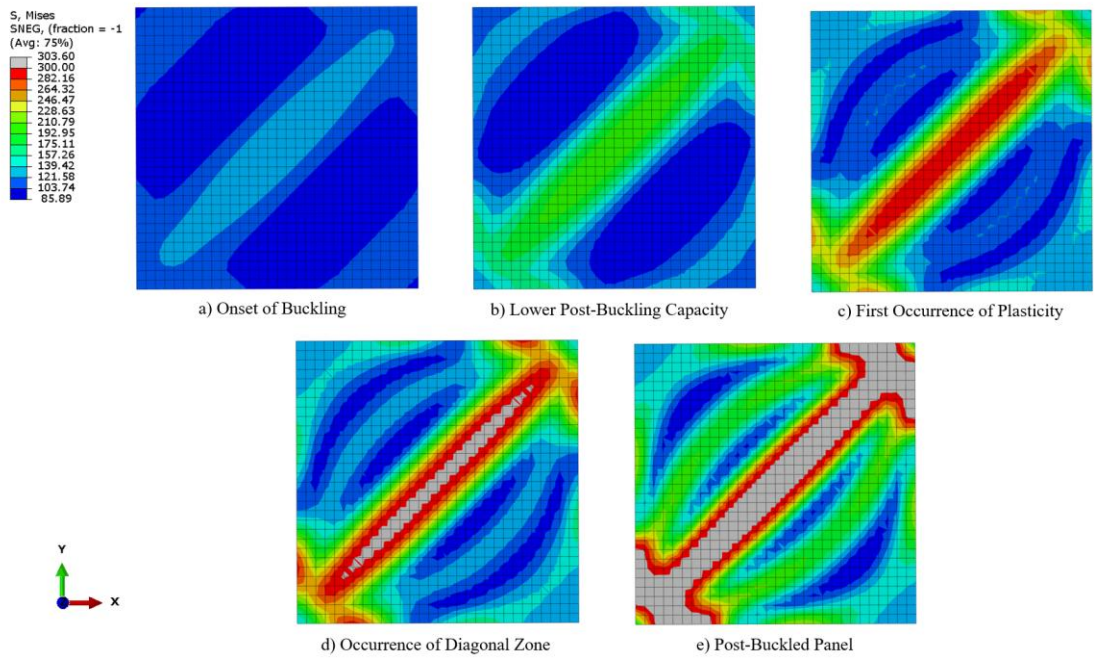

Figure 5.2 : Stress plots of ST37-750X750X3 for different stages.

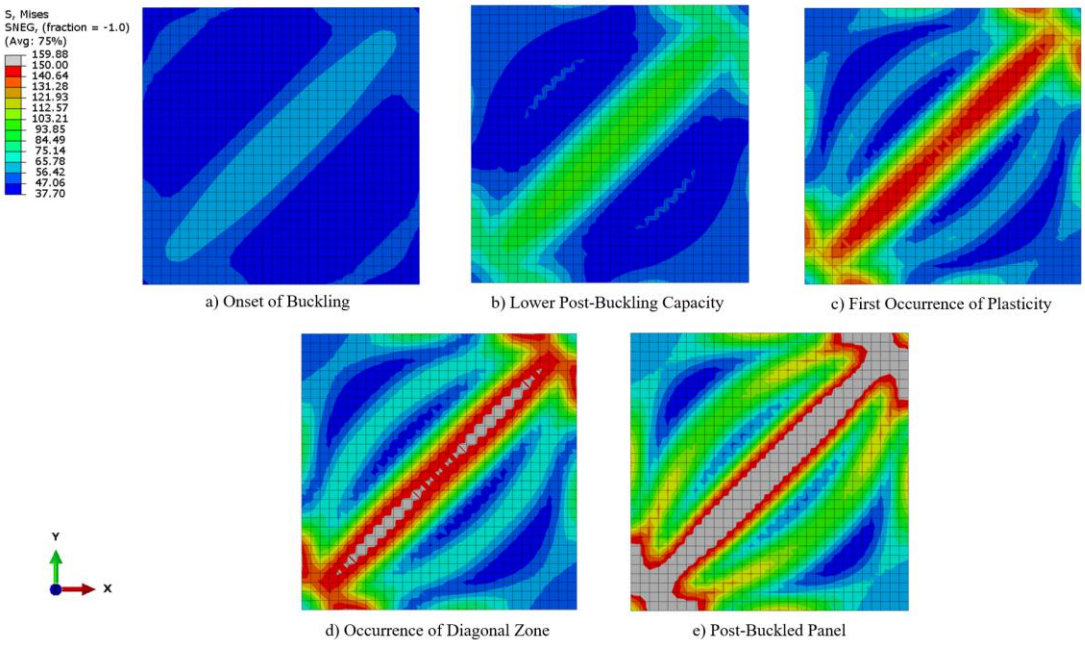

Figure 5.3 : Stress plots of AL57-750X750X3 for different stages.

The ultimate buckling loads are affected by the panel thickness, material properties, and size. Panels with higher thickness and stiffer materials such as ST-37 show higher ultimate loads and more stable post-buckling behavior but lower post-buckling reserve which is the ratio of the ultimate buckling load and the critical buckling load. On the other hand, thinner panels with softer materials like AL-5754 reach lower ultimate loads and show more deformation and higher post-buckling reserve.

The calculated ultimate buckling loads (F_U) and their F_U/F_{CR} ratios for all 18 panel models are presented in Table 5.4 and Table 5.5. As seen in the table, both the material type and the geometry of the panels (size and thickness) have a significant effect on the results. Steel panels, which has a higher Young's modulus, generally have higher F_U values compared to aluminum panels. However, their F_U/F_{CR} ratios are lower in some cases because their critical buckling loads are also high.

When thickness is compared, it can be seen that thinner panels (such as 2 mm) show higher F_U/F_{CR} ratios. For example, the AL57-750x750x2 panel has 3.64 F_U/F_{CR} ratio which is the highest ratio, showing that the panel can carry approximately 3.5 times bigger load after initial buckling. This indicates that thin and slender panels show a wider post-buckling behavior. On the other hand, thicker panels (like 4 mm) have smaller F_U/F_{CR} ratios, meaning that they reach their ultimate buckling load closer to their critical buckling load, with less post-buckling reserve.

Table 5.4 : The ultimate buckling loads aluminum panels.

Materials	F_U (N)	F_U/F_{CR}
AL57-500x500x2	34619.1	2.29
AL57-500x500x3	75144.5	1.47
AL57-500x500x4	132161.0	1.1
AL57-650x650x2	35825.8	3.08
AL57-650x650x3	76907.6	1.96
AL57-650x650x4	133838.6	1.44
AL57-750x750x2	36699.4	3.64
AL57-750x750x3	77892.0	2.29
AL57-750x750x4	134581.1	1.67

Table 5.5 : The ultimate buckling loads steel panels.

Materials	F_U (N)	F_U/F_{CR}
ST37-500x500x2	82452.5	1.83
ST37-500x500x3	180808.6	1.19
ST37-500x500x4	334562.9	0.93
ST37-650x650x2	84589.4	2.44
ST37-650x650x3	183608.4	1.57
ST37-650x650x4	321339.7	1.16
ST37-750x750x2	86237.7	2.87
ST37-750x750x3	185520.8	1.83
ST37-750x750x4	324232.9	1.35

Among the materials, AL-5754 panels show the highest F_U/F_{CR} ratios overall, especially for slender configurations thanks to its higher yield stress and lower elastic

modulus compared with AL-5754 alloy and ST-37. The ST-37 panels show the highest absolute F_U values due to their material strength, but their post-buckling reserve is more limited in some cases due to its higher elastic modulus and the critical buckling load.

This table shows that both material selection and geometric parameters have a strong effect on the post-buckling strength and reserve capacity. Also, these values are used in the next steps to study how plastic strain affects secondary buckling behavior.

5.4 Secondary Buckling Result

In this section, the secondary buckling behavior of the panels was investigated. This analysis was conducted using plastic strains in the post-buckling stage. To study the effect of plastic strain on the critical buckling load during reloading, four levels of plastic strain were applied: 25%, 50%, 75%, and 100% of the total strain that occurs at the ultimate buckling load.

To perform this analysis, the plastic strains from the post-buckling stage were defined using the Predefined Field feature in Abaqus. The simulation was solved in two steps. In the first step, the elastic strains were released to isolate the plastic strain effect. Then, a linear buckling analysis was performed using the Lanczos eigenvalue solver. The new critical buckling load, calculated with the presence of plastic strain, was called the secondary critical buckling load. They are depicted in Table 5.6, Table 5.7, Figure 5.4, Figure 5.5 and Figure 5.6.

The secondary buckling loads and percentage of reduction of critical buckling load of AL-5754 alloy panels for different plastic strain levels are presented in Table 5.6 and Figure 5.4. The results show that the buckling resistance is reduced in occurrence of plastic strain for all panel configurations due to the critical buckling load decreases as the applied plastic strain increases

For example, the critical buckling load of AL57-500×500×2 panel (-15.117 kN) shows about 10.7% reduction and the secondary buckling load is calculated as −13.5 kN when 100% plastic strain is applied. A similar trend is observed in larger and thicker panels like AL57-750×750×4 with about 4.1% decrease. Although this reduction seems smaller in percentage, it proves that plasticity brings a loss in structural stiffness.

When the effect of slenderness ratio is investigated for the panels with the same thickness, it is observed that the percentage reduction in the secondary buckling load increases as the slenderness ratio increases. For example, the reductions for AL57-500×500×2, AL57-650×650×2 and AL57-750×750×2 panels are calculated under 100% plastic strain as 10.7%, 29.5% and 48.9%, respectively. It can also be concluded from Table 5.6 that a similar relationship between panel length and the reduction in secondary buckling load is observed for panels with 3 mm and 4 mm thicknesses.

When the reduction of secondary buckling load is investigated for panels with same side length but different thicknesses, it can be said that the percentage of reduction decreases as the thickness increases.

Table 5.6 : The secondary buckling loads AL-5754 alloy panel.

Panels	Secondary Buckling Load (N)				
	0%	25%	50%	75%	100%
AL57-500x500x2	-15117.5	-14962.0	-14320.0	-13709.5	-13500.5
AL57-500x500x3	-50980.0	-50860.0	-50200.0	-49574.5	-49442.0
AL57-500x500x4	-120695.0	-120620.0	-120330.0	-119675.0	-119010.0
AL57-650x650x2	-11631.8	-11340.6	-10607.4	-9235.2	-8196.5
AL57-650x650x3	-39238.6	-38983.8	-37713.0	-36902.5	-36728.9
AL57-650x650x4	-92943.5	-92755.0	-91695.5	-90616.5	-90278.5
AL57-750x750x2	-10082.3	-9616.5	-8769.0	-6761.7	-5151.4
AL57-750x750x3	-34014.0	-33664.5	-32236.5	-30846.8	-30375.8
AL57-750x750x4	-80587.5	-80280.0	-78690.0	-77400.0	-77310.0

The Figure 5.4 shows the percentage reduction in secondary buckling load of AL-5754 alloy panels for different percentage of applied strain in detail. For instance, when 25% plastic strain is applied on the AL57-650×650×2 panel configuration, 2.5% reduction of secondary buckling load is occurred. While applying 50% plastic strain causes 8.8% reduction, 20.6% reduction is caused by applying 75% plastic strain. Application of 100% plastic strain gives the occurred maximum reduction of 29.5% for the AL57-

650×650×2 panel configuration. It can be said that reduction increases as increasing applied strain.

As can be seen from Figure 5.4, the maximum reduction occurs in the AL57-750×750×2 panel for each level of applied plastic strain. Conversely, the minimum reduction is observed in the AL57-500×500×4 panel in every plastic strain level. This relationship clearly indicates a direct correlation between the slenderness ratio and the percentage of reduction.

Smaller reductions for all plastic strain level are calculated for thicker panels such as AL57-750×750×4 or AL57-500×500×4 panel configuration. As an example, while only 1.4% reduction is calculated for the AL57-500×500×4 panel configuration when 100% plastic strain is applied, 25% plastic strain causes 0.06% reduction. Also, reduction for AL57-750×750×4 are calculated as 0.4% and 4.1% under 25% and 100% plastic strain, respectively. These values mean that thicker panels are mostly preserved their stiffness and they resist post-buckling weakening better than thinner ones, regardless of the level of applied plastic strain.

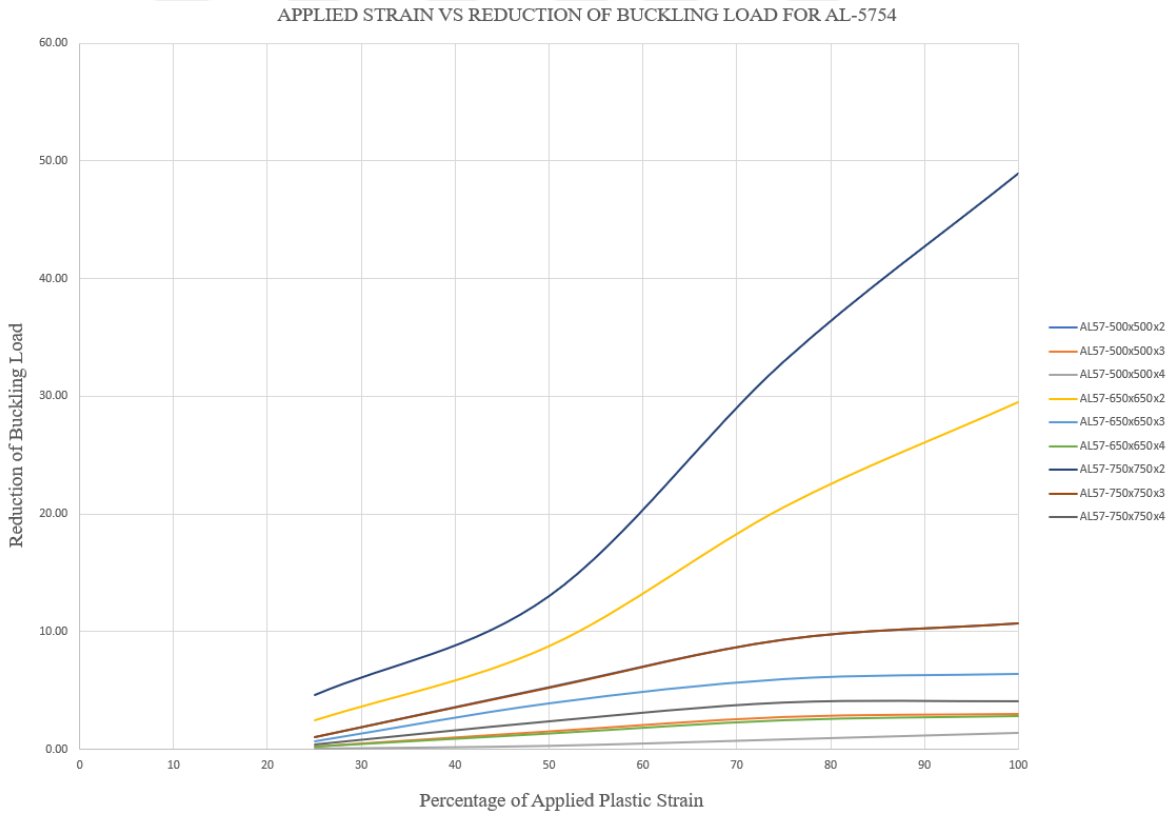

Figure 5.4 : Applied strain vs reduction of secondary buckling load for AL-5754.

Table 5.7 presents the secondary buckling loads of ST-37 steel panels for 0%, 25%, 50%, 75%, and 100% applied plastic strain. The results show that plastic strain causes a small reduction in critical buckling loads, especially when compared to aluminum panels.

For example, in the ST37-500×500×2 panel, the buckling load drops from −45.056 kN to −42.593 kN, which is about 5.5% reduction. The ST37-500×500×4 panel shows smaller reduction. It reduces from −359.745 kN to −359.715 N with only 0.008% difference under 100% plastic strain. This result confirms that thicker steel panels are very resistant to plastic strain effects like aluminum panels, and their stiffness is almost fully preserved after deformation.

When comparing different sizes, the ST37-750×750×2 panel shows a larger drop (about 22.9%) from −30.0 kN to −23.16 kN, indicating that slender and thin panels are more sensitive to plastic strain even for high-strength steel materials. However, even in these cases, the reduction is still lower than what is observed in thinner aluminum panels.

Table 5.7 : The secondary buckling loads ST-37 panel.

Panels	Secondary Buckling Load (N)				
	0%	25%	50%	75%	100%
ST37-500x500x2	-45056.0	-44839.0	-43731.5	-42911.0	-42593.5
ST37-500x500x3	-151940.0	-151875.0	-151515.0	-150650.0	-149830.0
ST37-500x500x4	-359745.0	-359745.0	-359735.0	-359720.0	-359715.0
ST37-650x650x2	-34667.8	-34258.9	-33082.4	-30966.0	-30085.3
ST37-650x650x3	-116948.0	-116623.0	-114861.5	-113178.0	-112807.5
ST37-650x650x4	-277017.0	-276809.0	-275905.5	-274046.5	-272402.0
ST37-750x750x2	-30048.0	-29477.3	-28164.8	-25437.8	-23160.0
ST37-750x750x3	-101378.0	-100890.0	-98392.5	-96547.5	-95835.
ST37-750x750x4	-240173.0	-239820.0	-237810.0	-235327.5	-234315.0

Figure 5.5 shows the percentage reduction in secondary buckling loads for ST-37 steel panels at different levels of applied plastic strain (25%, 50%, 75%, and 100%). These values reflect how much buckling capacity decreases after plastic deformation. It can be observed that percentage of reduction of secondary buckling is proportional with applied strain like AL-5754 alloy. However, ST-37 panels are less sensitive to plastic strain especially in thicker configurations due to its lower post-buckling reserve.

For example, when the reduction of secondary buckling load of ST37-500×500×4 panel under four different applied strain, it can be concluded that plastic strain has almost no effect on its buckling performance. Similarly, ST37-500×500×3 panel configuration shows a very small reduction of 0.04%, 0.3%, 0.85% and 1.4% for 25%, 50%, 75% and 100% plastic strain, respectively. These confirm that thicker steel panels maintain their stiffness even after undergoing plastic deformation.

On the other hand, more slender and thinner panels demonstrate greater sensitivity to plastic strain. ST37-750×750×2 panel configuration which has the highest calculated reduction among the ST-37 panel configurations under 100% plastic strain has 1.9%, 6.3% and 15.3% reductions under 25%, 50% and 75% applied plastic stain, respectively. When the reduction values of ST37-650×650×2 panel are also investigated, it can be said that the percentage reduction decreases with decreasing side length of panel like in aluminum panels.

Overall, for every applied plastic strain, the reduction in secondary buckling load becomes more visible in panels with higher slenderness ratio. For instance, whereas the reduction of secondary buckling load of panel has 250 slenderness ratios is 4.8%, the panel with a slenderness ratio of 375 shows a 15.3% reduction when 75% plastic strain is applied. Additionally, while there is no effect of plastic strain for the panel has 125 slenderness ratio, 4.6% reduction is calculated for the panel with 325 slenderness ratio under 50% plastic strain.

Figure 5.6 clearly illustrates the comparison between the percentage reduction in secondary buckling loads for AL-5754 and ST-37 panels and different slenderness ratios. It can be observed that there is a direct relationship between the slenderness ratio (β) and the reduction of buckling load for both materials.

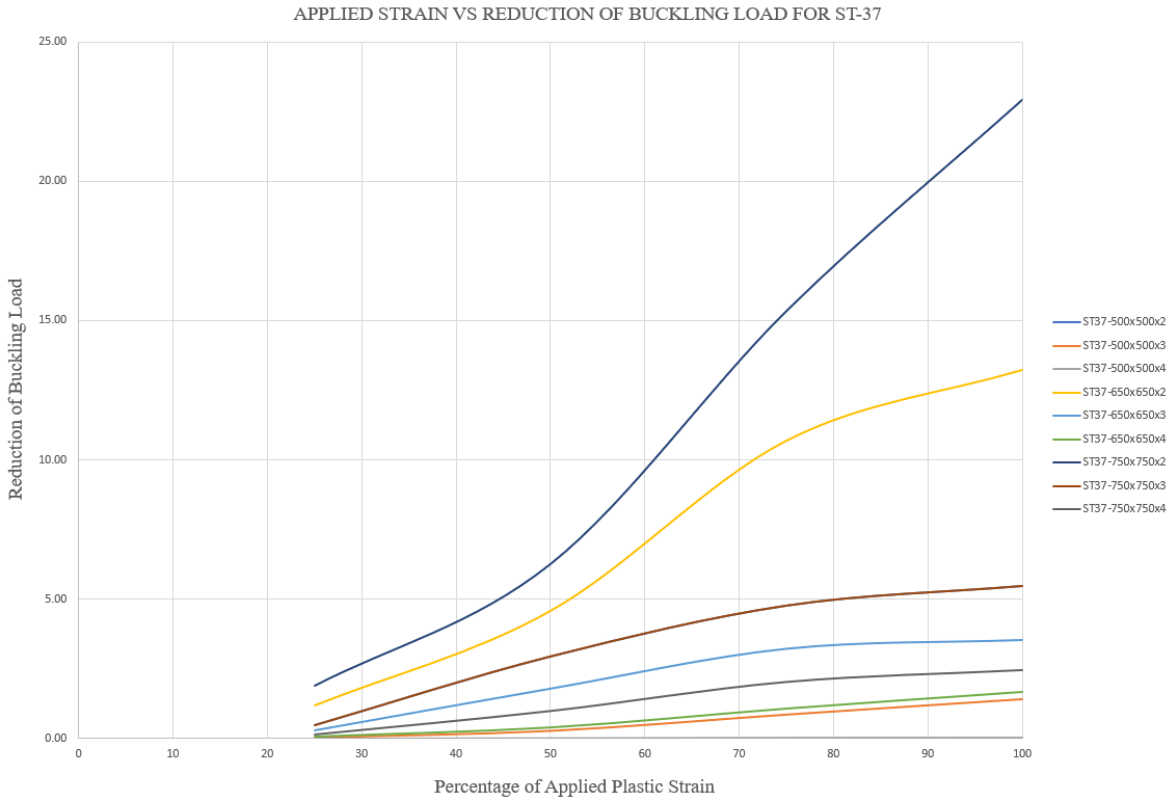

Figure 5.5 : Applied strain vs reduction of secondary buckling load for ST-37.

At low slenderness ratios, both AL-5754 and ST-37 show very small reductions in buckling load, even under 100% plastic strain. This indicates shorter and thicker panels are more resistant to plastic strain. However, as the slenderness ratio increases, the reduction becomes much higher especially for AL-5754.

Moreover, it can be seen from the figure that the reduction of buckling load is calculated the same for the 750X750X3 mm and 500X500X2 mm panel configurations. The common property of these panels is their slenderness ratio and post-buckling reserve, which directly affect the percentage reduction in buckling load.

While the reduction for ST-37-500×500×2 panel configuration increases gradually from 0.5% at 25% strain to 5.5% at 100%, the AL-5754 panel of the same size shows 1.03% at 25%, and 10.7% reduction is calculated when 100% plastic strain is applied, which means that the aluminum panels loses their stiffness than steel plates under the same conditions.

ST-37-500×500×3 panel shows only 1.4% reduction at 100% strain, while the reduction of secondary buckling load of AL-5754 reaches more than twice as much, which is 3.02%. In 500×500×4 panels, there is almost no reduction for the ST-37 panel,

while AL-5754 still shows a larger reduction under 100% plastic strain. The calculated reductions are 0.008% and 1.4% for the AL-5754 and ST-37, respectively. These results clearly show that thicker steel panels are nearly unaffected, while aluminum still loses some strength.

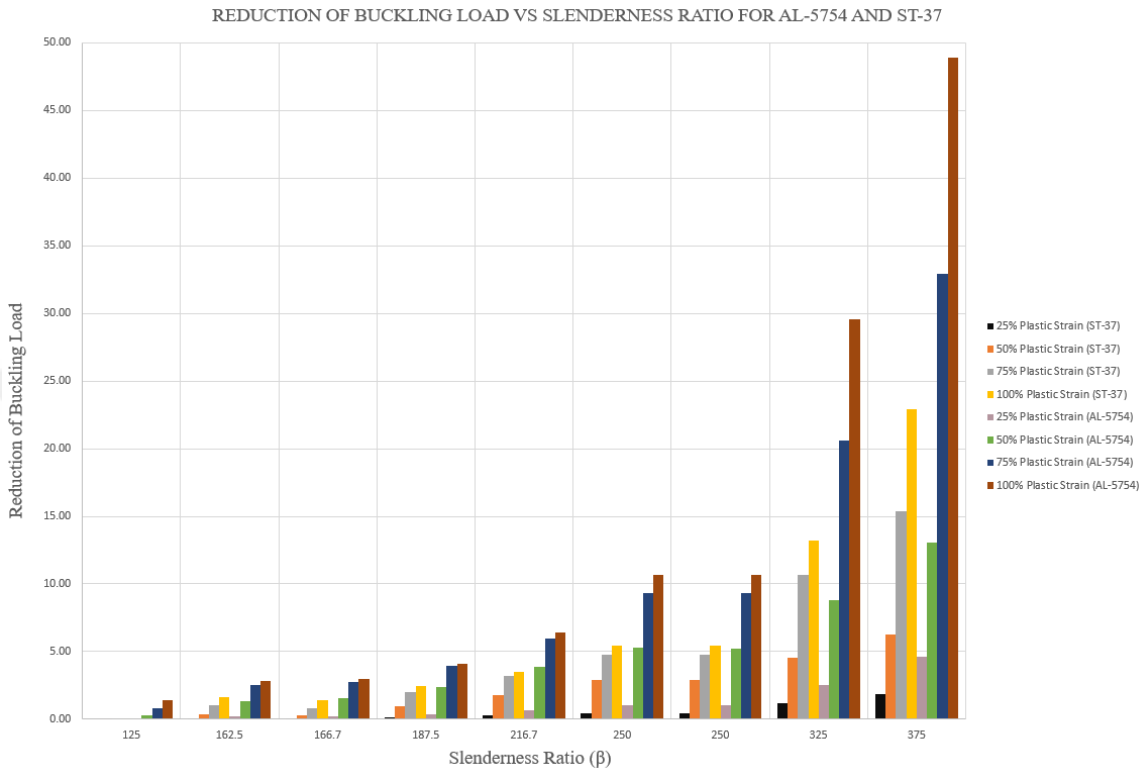

Figure 5.6 : Slenderness ratio (β) vs applied strain for AL-5754 and ST-37.

The difference becomes even clearer as the slenderness ratio increases. The reductions of 650×650×2 panels are calculated as 13.2% and 29.5% at 100% strain for the ST-37 and AL-5754, respectively. These reductions are decreased with increasing thickness. However, the aluminum panels always show higher reduction compared to steel panel even in same slenderness ratio. For example, 3.5% and 6.4% values are calculated for 650×650×3, and 1.6% and 2.9% values are calculated for 650×650×4 panel configurations for ST-37 and AL-5754 materials, respectively.

The biggest difference is seen in 750×750×2 panels, where the ST-37 panel reduces by 22.9%, but AL-5754 drops sharply by 48.9%, showing that thin and large aluminum panels lose nearly half of their buckling strength under full plastic strain. In the 750×750×3 configuration, ST-37 shows 5.5%, while AL-5754 shows 10.7%. Even in 750×750×4 panels, ST-37 shows 2.4% and AL-5754 has 4.07%.

These values show that ST-37 steel is more resistant to buckling strength reduction after plastic strain, especially in thicker or shorter panels. In contrast, AL-5754 panels are more sensitive and can lose a significant part of their capacity, especially when thin and slender.

6. CONCLUSION

In this study, the effects of plastic strain on the critical buckling behavior of slender panels under in-plane shear loading were investigated. Both numerical analysis and experimental study were used to understand influence of plastic strain, developed in the post-buckling stage, on the critical buckling load during reloading.

The results showed that as plastic strain increases, the secondary buckling load decreases. This effect becomes more significant in panels with higher slenderness ratios and smaller thicknesses. In general, slender and thin panels are more sensitive to plastic strain, while thicker and shorter panels preserve most of their buckling strength.

When different materials were compared, ST-37 panels performed better than AL-5754 panels in terms of resistance to plastic strain. For example, at 100% plastic strain, the AL-5754 panel with a slenderness ratio of 375 showed up to 48.9% reduction, while the ST-37 panel of the same size showed only 33% reduction.

Among the materials, panels made from ST-37 show the least sensitivity to plastic stain especially for panels with 4 mm thickness, which maintain nearly their full buckling capacity with less than 2% reduction.

The findings confirm that both material selection and geometric properties (slenderness ratio and thickness) have a strong influence on secondary buckling load of panel and their post-buckling performance. For structural applications where panels may undergo plastic deformation and be reloaded, ST-37 is a more reliable material for designs requiring high stability and load-carrying capacity after buckling. especially in shorter and thicker forms. This makes ST37 a good choice for structures that may experience overloading or reloading conditions.

This research helps improve understanding of change of critical buckling load due to plastic strain and offers valuable data for the design and reusability of metal panels in aerospace, civil, and mechanical engineering applications.

REFERENCES

[1] Paul, A., & George, S. P. (2014). Buckling analysis of wing upper skin panels of a transport aircraft. *International Journal of Science, Engineering and Technology Research (IJSETR)*, *3*(10), 2868-2872.

[2] Nwoji, C. U., Onah, H. N., Mama, B. O., Ike, C. C., & Ikwueze, E. U. (2017). Elastic buckling analysis of simply supported thin plates using the double finite Fourier sine integral transform method. *Explorematics Journal of Innovative Engineering and Technology*, *1*(1), 37-47.

[3] Timoshenko, S. P., & Gere, J. M. (2012). *Theory of elastic stability*. Courier Corporation.

[4] Timoshenko, S. P., Gere, J. M., & Prager, W. (1962). Theory of Elastic Stability, Second Edition. *Journal of Applied Mechanics*, *29*(1), 220–221. https://doi.org/10.1115/1.3636481

[5] Bulson, P. S. (1970). The stability of flat plates. *(No Title)*.

[6] Yu, C. (2003). Buckling of rectangular plates under intermediate and end loads.

[7] Gerard, G., & Becker, H. (1957). Handbook of structural stability. Pt. 3. Buckling of curved plates and shells. Washington: NACA.

[8] Ferri, A., Nowick, A. S., Budiansky, B., Garrick, I. E., Sivells, J. C., Dawson, J. R., ... & Hay, E. S. (1946). Critical Combinations of Shear and Transverse Direct Stress for an Infinitely Long Flat Plate with Edges Elastically Restrained Against Rotation (No. 841-850). US Government Printing Office.

[9] Batdorf, S. B., & Stein, M. (1947). Critical combinations of shear and direct stress for simply supported rectangular flat plates (No. NACA-TN-1223).

[10] Johnson Jr, A. E., & Buchert, K. P. (1951). Critical combinations of bending, shear, and transverse compressive stresses for buckling of infinitely long flat plates (No. NACA-TN-2536).

[11] Kang, J. H., & Leissa, A. W. (2001). Vibration and buckling of SS-F-SS-F rectangular plates loaded by in-plane moments. *International journal of structural stability and dynamics*, *1*(04), 527-543.

[12] Xiang, Y., Wang, C. M., & Wang, C. (2001). Buckling of rectangular plates with internal hinge. *International journal of structural stability and dynamics*, *1*(02), 169-179.

[13] Xiang, Y., Wang, C. M., Wang, C. Y., & Su, G. H. (2003). Ritz buckling analysis of rectangular plates with internal hinge. *Journal of engineering mechanics*, *129*(6), 683-688.

[14] Gheitasi, A., & Alinia, M. (2010). Slenderness classification of unstiffened metal plates under shear loading. *Thin-Walled Structures*, *48*(7), 508–518. https://doi.org/10.1016/j.tws.2010.02.004

[15] Amani, M., Alinia, M., & Fadakar, M. (2013). Imperfection sensitivity of slender/stocky metal plates. *Thin-Walled Structures*, *73*, 207–215. https://doi.org/10.1016/j.tws.2013.08.010

[16] Ghadami, A., & Broujerdian, V. (2019). Shear behavior of steel plate girders considering variations in geometrical properties. *Journal of Constructional Steel Research*, *153*, 567–577. https://doi.org/10.1016/j.jcsr.2018.11.009

[17] Elgaaly, M. (2000). Post-buckling behavior of thin steel plates using computational models. *Advances in Engineering Software*, *31*(8–9), 511–517. https://doi.org/10.1016/s0965-9978(00)00037-5

[18] Cheng, H. S., Cao, J., & Wang, H. P. (2006, January). Experimental and numerical analysis of the buckling and post-buckling phenomenon in the Yoshida test. In *International Manufacturing Science and Engineering Conference* (Vol. 47624, pp. 249-256).

[19] Rasool, M., & Singha, M. (2016). A finite element study on the nonlinear behavior of rectangular shear panels. *Thin-Walled Structures*, *104*, 248–258. https://doi.org/10.1016/j.tws.2016.03.022

[20] Ljubinković, F., Martins, J. P., & Simões da Silva, L. (2017). Cylindrically curved steel panels in bridge design: Buckling and post-buckling behaviour under shear stresses. In *Proceedings of Eurosteel 2017, Copenhagen, Denmark* (pp. 1-12). Ernst & Sohn Verlag.

[21] Amani, M., Edlund, B., & Alinia, M. M. (2011). Buckling and postbuckling behavior of unstiffened slender curved plates under uniform shear. *Thin-Walled Structures*, *49*(8), 1017–1031. https://doi.org/10.1016/j.tws.2011.03.007

[22] Park, J. S., & Seo, J. K. (2015). Analytical method for simulation of buckling andPost-buckling behaviour of curved pates. *Computer Modeling in Engineering & Sciences*, *106*(4), 291–308. https://doi.org/10.3970/cmes.2015.106.291

[23] Melcon, M. A., & Ensrud, A. F. (1953). Analysis of stiffened curved panels under shear and compression. *Journal of the Aeronautical Sciences*, *20*(2), 111-119.

[24] Lee, S. C., & Yoo, C. H. (1999). Experimental study on ultimate shear strength of web panels. *Journal of Structural Engineering, 125*(8), 838-846. https://doi.org/10.1061/(ASCE)0733-9445(1999)125:8(838)

[25] Xiao, Y., Xue, X. Y., Sun, F. F., & Li, G. Q. (2018b). Postbuckling shear capacity of high-strength steel plate girders. *Journal of Constructional Steel Research*, *150*, 475–490. https://doi.org/10.1016/j.jcsr.2018.08.032

[26] Yuan, L., Zhang, Q., Luo, X., Ouyang, Y., & Yin, J. (2021). Shear resistance of aluminum alloy extruded H-Section beams. *Thin-Walled Structures*, *159*, 107219. https://doi.org/10.1016/j.tws.2020.107219

[27] Ibrahim, M. M., Aghoury, I. M. E., & Ibrahim, S. A. (2020). Experimental and numerical investigation of ultimate shear strength of unstiffened

slender web-tapered steel members. *Thin-Walled Structures*, *148*, 106601. https://doi.org/10.1016/j.tws.2020.106601

[28] Cricrì, G., Perrella, M., & Calì, C. (2014). Experimental and Numerical Post-buckling Analysis of Thin Aluminium Aeronautical Panels under Shear Load. *Strain*, *50*(3), 208–222. https://doi.org/10.1111/str.12083

[29] Hussain, N., & Loughlan, J. (2018, July). Buckling and post-buckling performance of stiffened webs subjected to interactive shear and compression. In *8th International conference on Thin-Walled Structures*.

[30] Featherston, C. A., Koffi, K., & Burguete, R. (2006). Postbuckling behaviour of a stiffened panel subject to combined loading. In *Proceedings of the 25th International Congress of the Aeronautical Sciences* (ICAS 2006)

[31] Alinia, M., & Shirazi, R. S. (2009). On the design of stiffeners in steel plate shear walls. *Journal of Constructional Steel Research*, *65*(10–11), 2069–2077. https://doi.org/10.1016/j.jcsr.2009.06.009

[32] Prato, A., Al-Saymaree, M., Featherston, C., & Kennedy, D. (2022). Buckling and post-buckling of thin-walled stiffened panels: modelling imperfections and joints. *Thin-Walled Structures*, *172*, 108938. https://doi.org/10.1016/j.tws.2022.108938

[33] Su, Y., Guan, Z., Wang, X., Li, Z., Guo, J., & Huang, Y. (2019). Buckling and post-buckling behavior of titanium alloy stiffened panels under shear load. *Chinese Journal of Aeronautics*, *32*(3), 619–626. https://doi.org/10.1016/j.cja.2018.09.007

[34] Basler, K. (1961). Strength of plate girders under combined bending and shear. *Journal of the Structural Division*, *87*(7), 181–198. https://doi.org/10.1061/jsdeag.0000698

[35] Glassman, J. D., & Garlock, M. E. M. (2016). A compression model for ultimate postbuckling shear strength. *Thin-Walled Structures*, *102*, 258–272. https://doi.org/10.1016/j.tws.2016.01.016

[36] Alinia, M., Habashi, H., & Khorram, A. (2008). Nonlinearity in the postbuckling behaviour of thin steel shear panels. *Thin-Walled Structures*, *47*(4), 412–420. https://doi.org/10.1016/j.tws.2008.09.004

[37] Garlock, M. E. M., Quiel, S. E., Yang, P. Y., Alos-Moya, J., & Glassman, J. D. (2019b). Post-Buckling mechanics of a square slender steel plate in pure shear. *Engineering Journal*, *56*(1), 27–46. https://doi.org/10.62913/engj.v56i1.1142

[38] Wang, P. Y., Masungi, P. M., Garlock, M. E., & Quiel, S. E. (2021). Postbuckling mechanics in slender steel plates under pure shear: A focus on boundary conditions and load path. *Thin-Walled Structures*, *169*, 108448. https://doi.org/10.1016/j.tws.2021.108448

[39] Gerard, G., & Becker, H. (1957). *HANDBOOK OF STRUCTURAL STABILITY. PART i. BUCKLING OF FLAT PLATES*. https://doi.org/10.2172/4343548

[40] Powell, G., & Simons, J. (1981). Improved iteration strategy for nonlinear structures. *International Journal for Numerical Methods in*

Engineering, *17*(10), 1455–1467. https://doi.org/10.1002/nme.1620171003

[41] Schenk, C. A., & Schuller, G. I. (2005). Uncertainty assessment of large finite element systems. In *Lecture notes in applied and computational mechanics*. https://doi.org/10.1007/11673941

[42] Kadapa, C. (2021). A simple extrapolated predictor for overcoming the starting and tracking issues in the arc-length method for nonlinear structural mechanics. *Engineering Structures*, *234*, 111755. https://doi.org/10.1016/j.engstruct.2020.111755

[43] Ghorbani-Menghari, H., Mohammadhosseinzadeh, M., Sarband, A. S., Wahabzadeh, A. H., Kahhal, P., & Kim, J. H. (2023). Investigation of the effects of process parameters on hydrodynamic deep drawing of AL-1050 sheet with indentations using genetic algorithm–based optimization. *The International Journal of Advanced Manufacturing Technology*, *129*(9–10), 3949–3964. https://doi.org/10.1007/s00170-023-12480-0

[44] Yang, Y., & Shieh, M. (1990). Solution method for nonlinear problems with multiple critical points. *AIAA Journal*, *28*(12), 2110–2116. https://doi.org/10.2514/3.10529

[45] Li, Y., Liu, F., & Cheng, W. (2021). Influence of lacing bars on the buckling capacity of four-legged latticed columns considering geometric imperfections. *Science Progress*, *104*(2), 003685042110259. https://doi.org/10.1177/00368504211025905

[46] Castro, S. G. P. (2015). Semi-analytical tools for the analysis of laminated composite cylindrical and conical imperfect shells under various loading and boundary conditions. https://doi.org/10.21268/20150210-154320

[47] Antoniou, S., & Pinho, R. (2018). Nonlinear seismic analysis of framed structures. In *CRC Press eBooks* (pp. 268–301). https://doi.org/10.1201/9781315119908-8

[48] Leon, S. E., Paulino, G. H., Pereira, A., Menezes, I. F. M., & Lages, E. N. (2011). A unified library of nonlinear solution schemes. *Applied Mechanics Reviews*, *64*(4). https://doi.org/10.1115/1.4006992

[49] Zlatanovic, D. L., Balos, S., Bergmann, J. P., Köhler, T., Grätzel, M., Sidjanin, L., & Goel, S. (2020). An experimental study on lap joining of multiple sheets of aluminium alloy (AA 5754) using friction stir spot welding. *The International Journal of Advanced Manufacturing Technology*, *107*(7–8), 3093–3107. https://doi.org/10.1007/s00170-020-05214-z

[50] Esmaeili, F., Rahmani, A., Barzegar, S., & Afkar, A. (2015). Prediction of fatigue life for multi-spot welded joints with different arrangements using different multiaxial fatigue criteria. *Materials & Design (1980-2015)*, *72*, 21–30. https://doi.org/10.1016/j.matdes.2015.02.008

APPENDICES

APPENDIX A: XY Strain Data of Panels up to Ultimate Buckling Load
APPENDIX B: XY Strain Data When Reloading of the Panels

APPENDIX A: XY Strain Data of Panels up to Ultimate Buckling Load

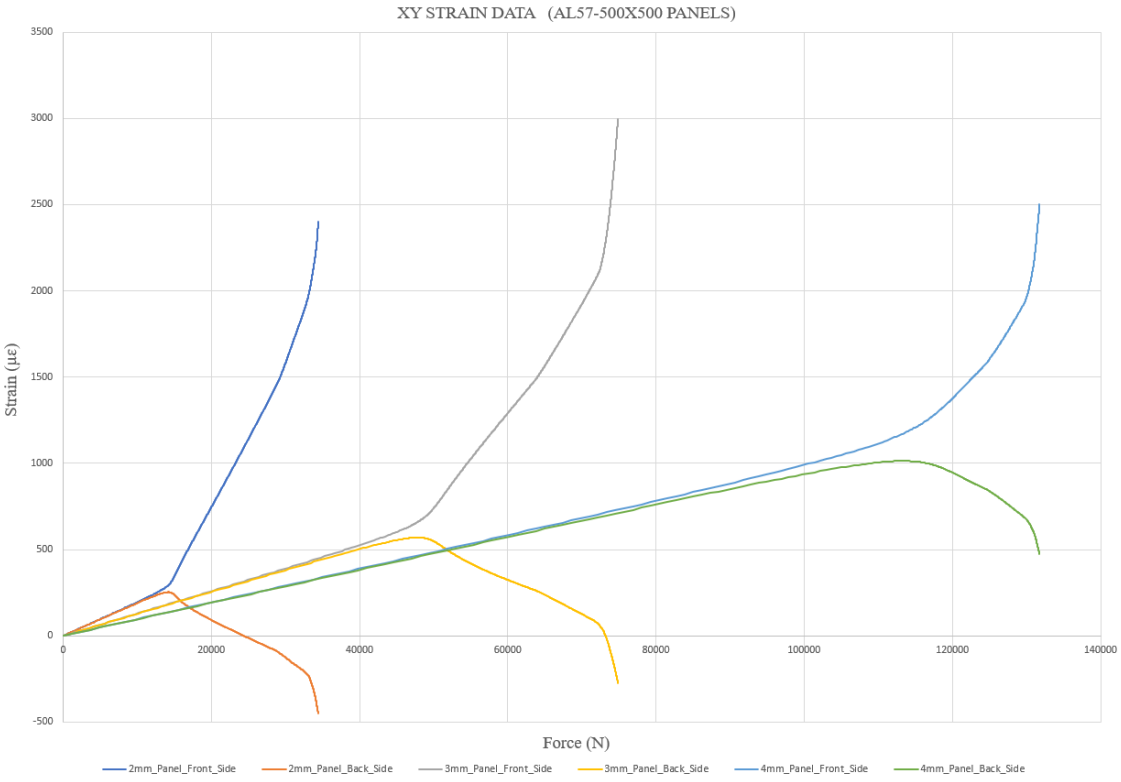

Figure A.1 : XY strain data of AL57-500X500 panel configurations.

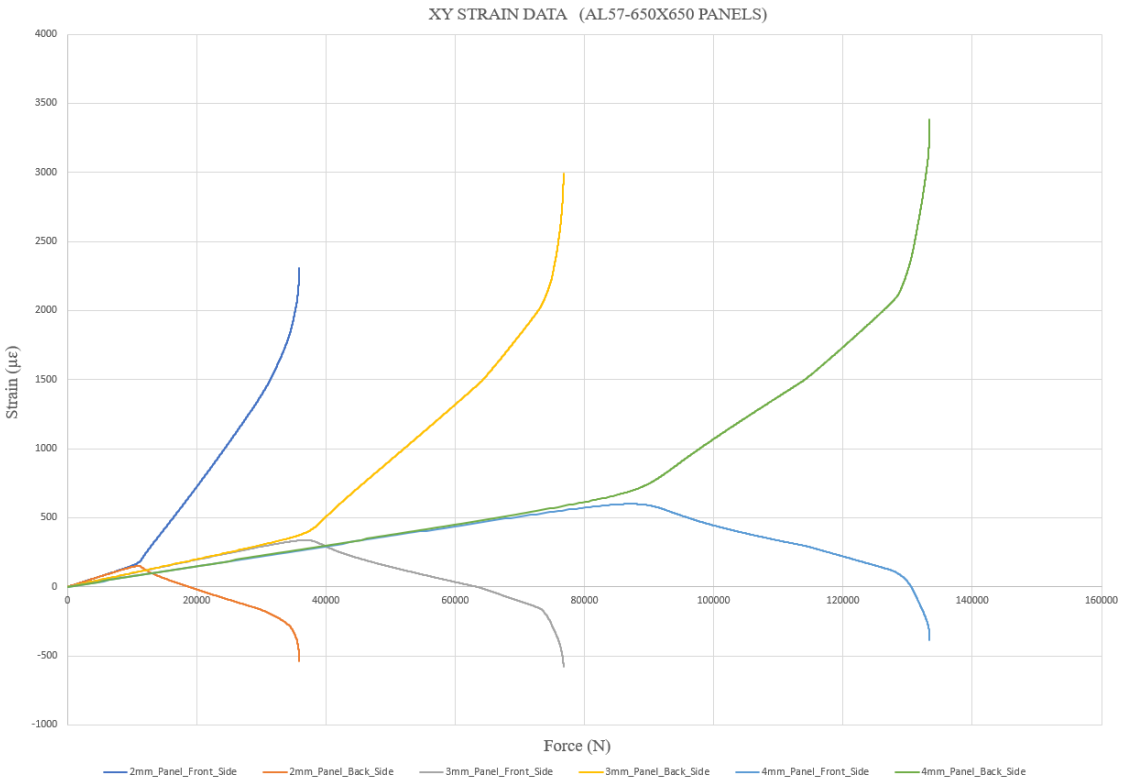

Figure A.2 : XY strain data of AL57-650X650 panel configurations.

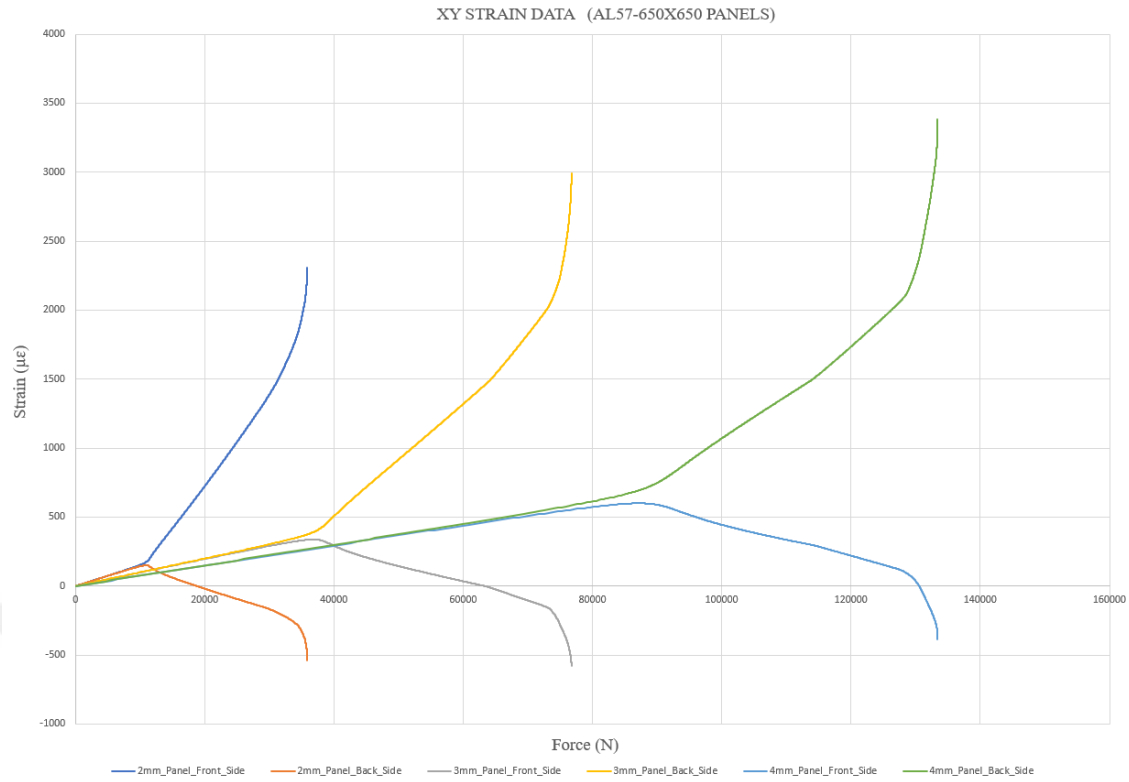

Figure A.3 : XY strain data of AL57-750X750 panel configurations.

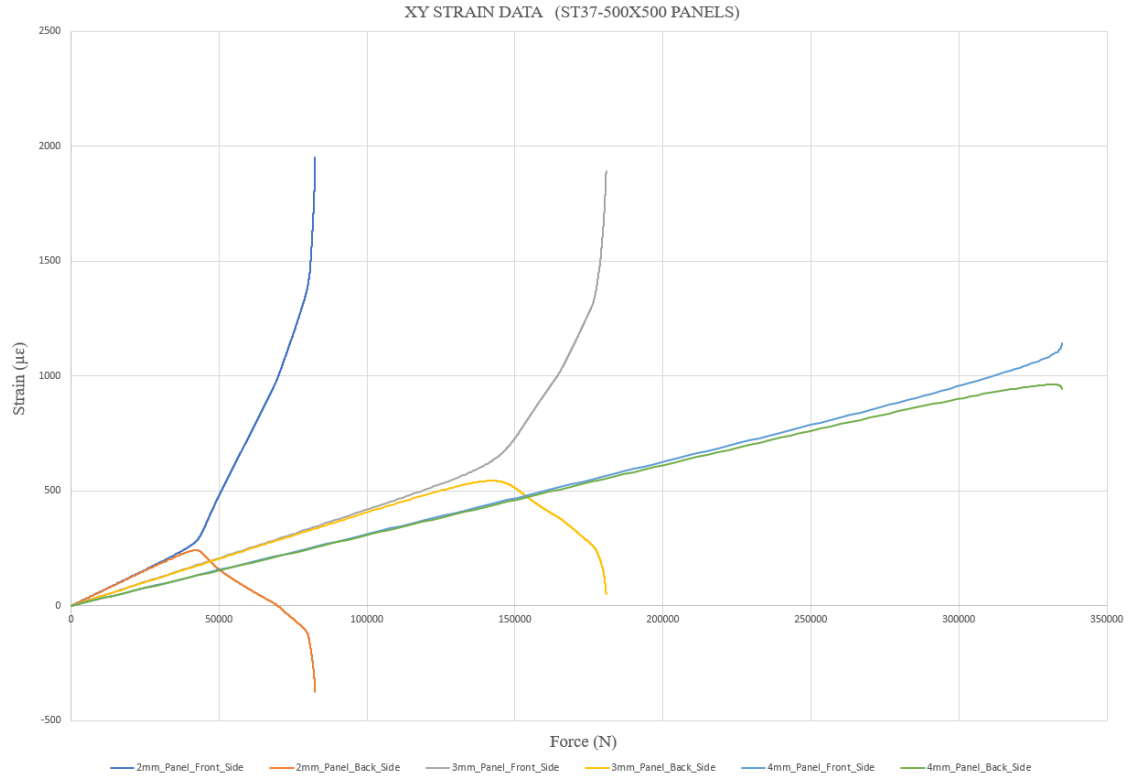

Figure A.4 : XY strain data of ST37-500X500 panel configurations.

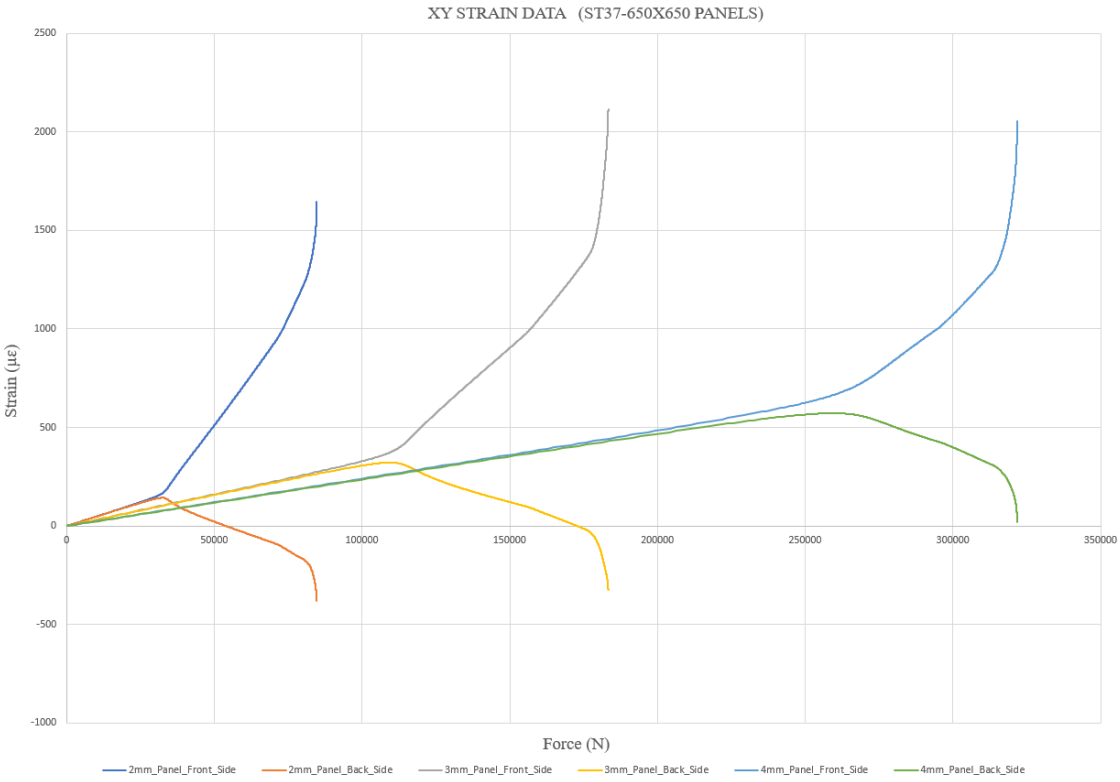

Figure A.5 : XY strain data of ST37-650X650 panel configurations.

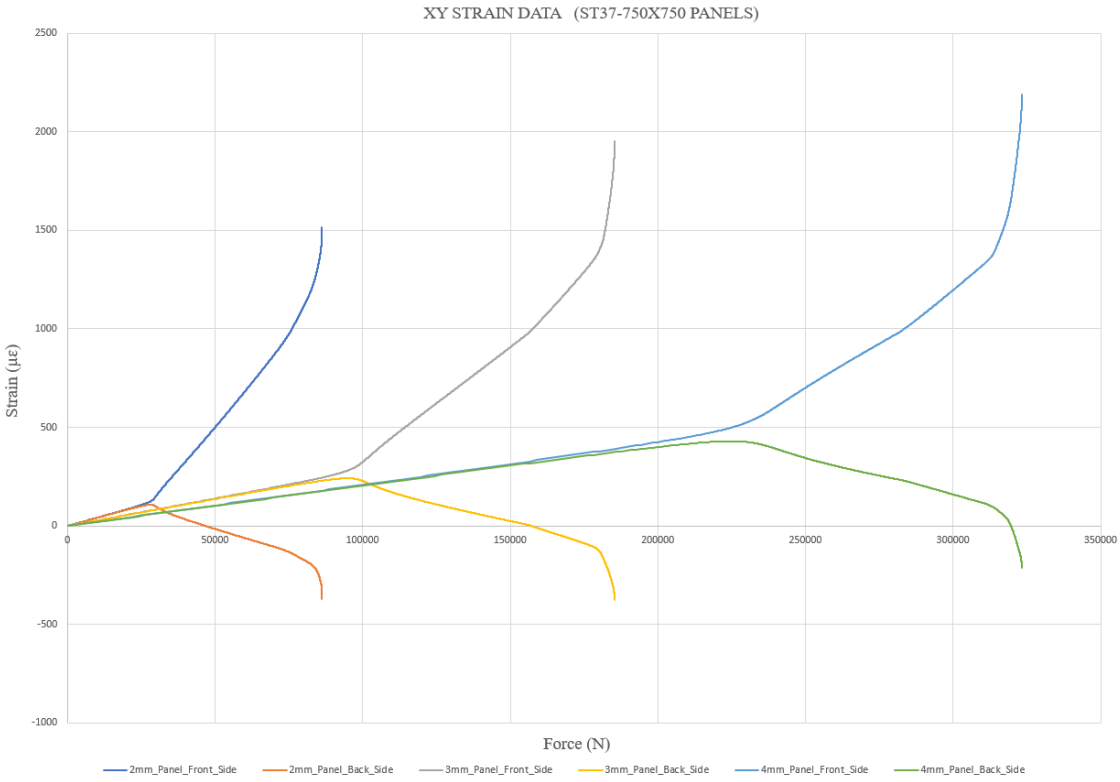

Figure A.6 : XY strain data of ST37-750X750 panel configurations.

APPENDIX B: XY Strain Data When Reloading of the Panels

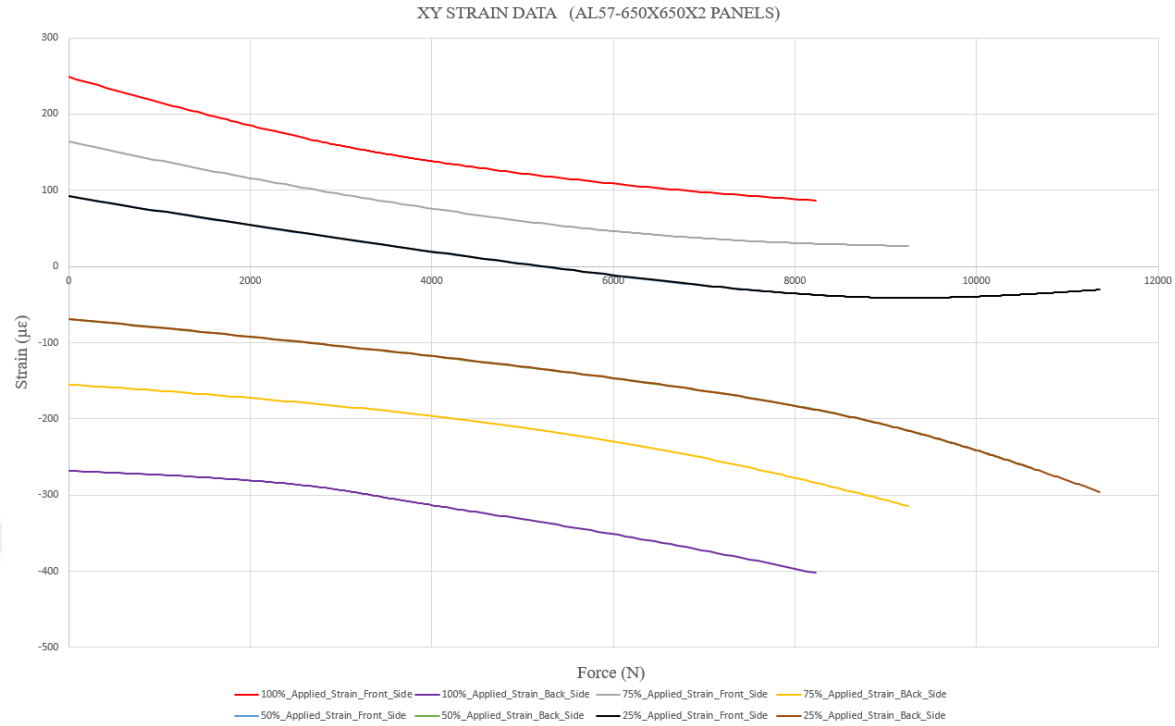

Figure B.1 : XY strain data of AL57-650X650X2 panel configuration.

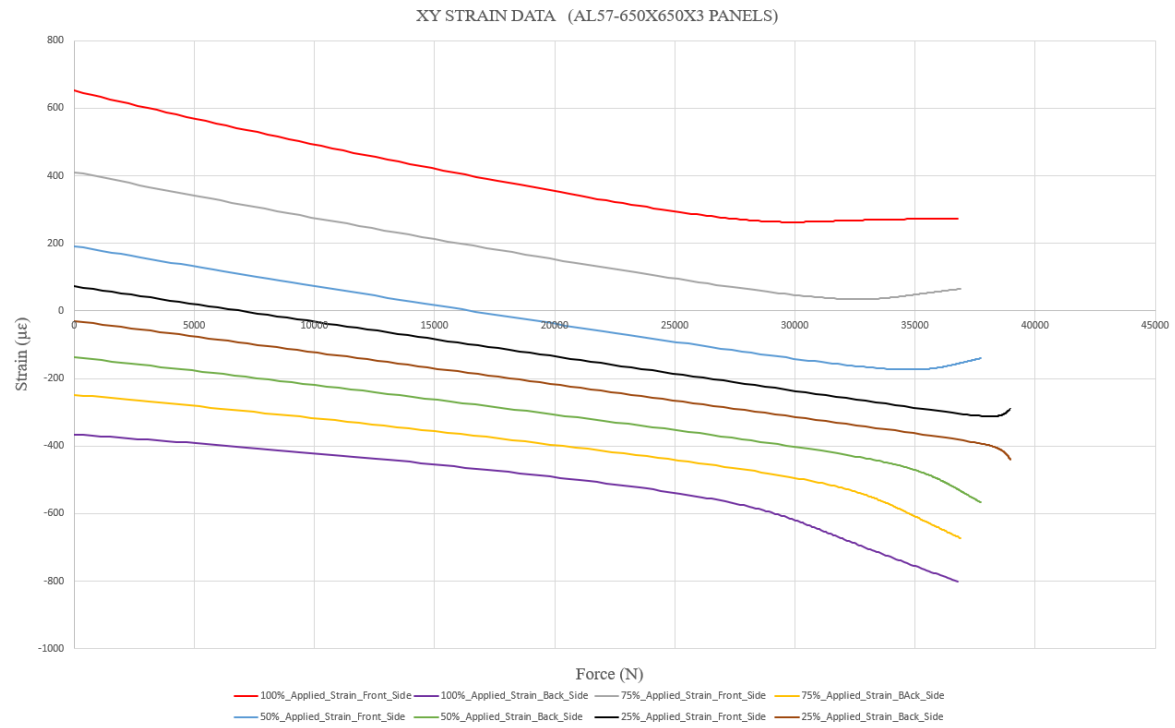

Figure B.2 : XY strain data of AL57-650X650X3 panel configuration.

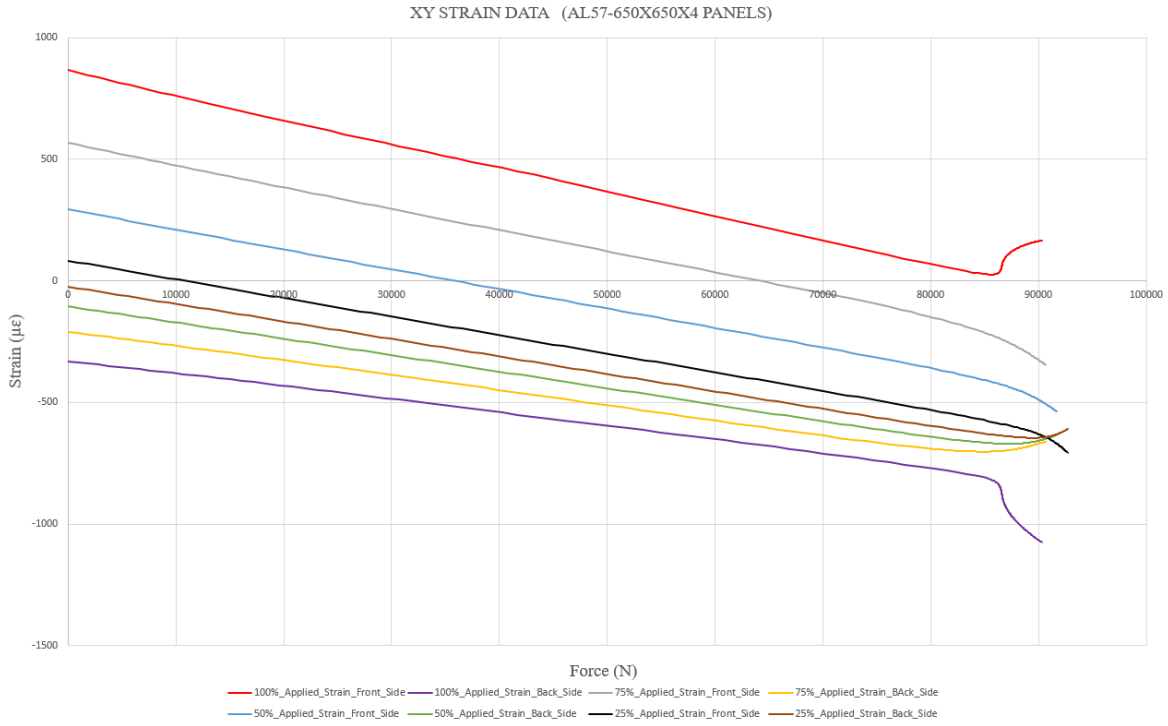

Figure B.3 : XY strain data of AL57-650X650X4 panel configuration.

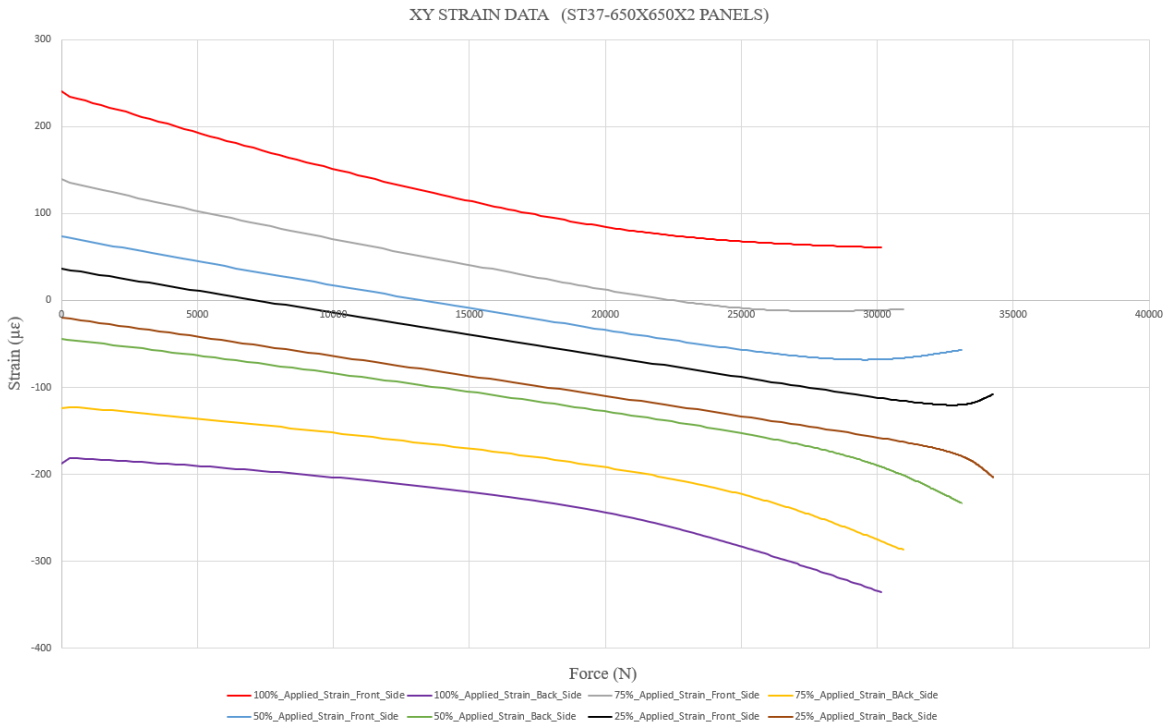

Figure B.4 : XY strain data of ST37-650X650X2 panel configuration.

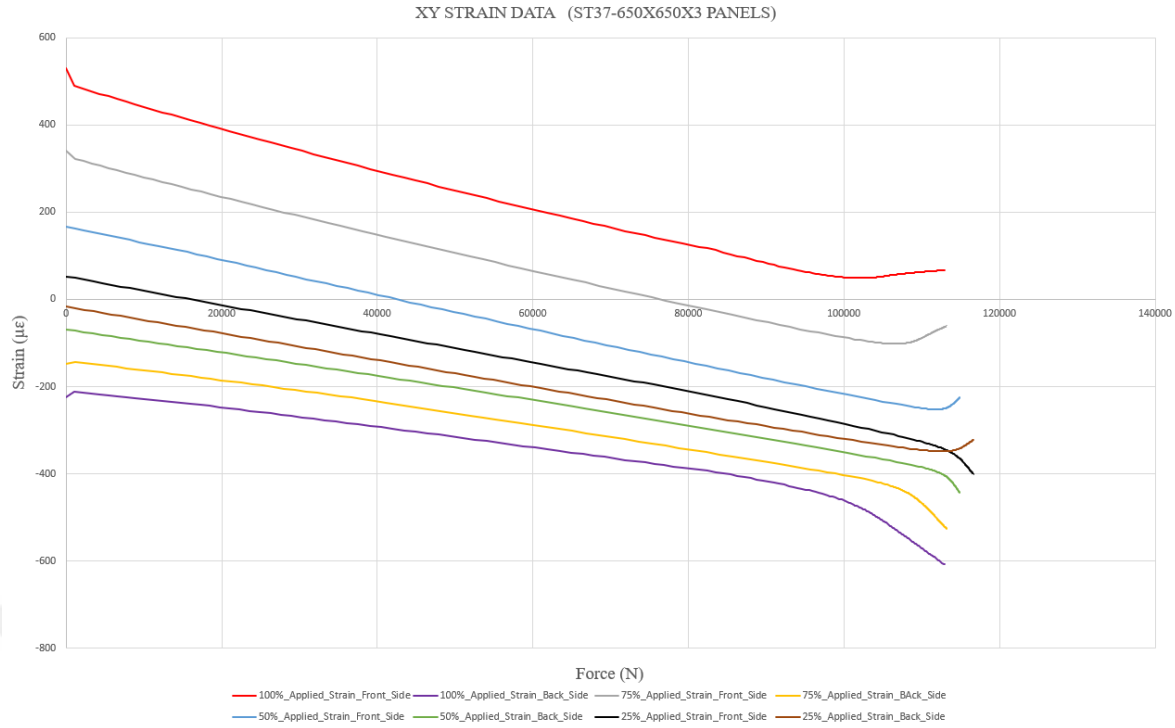

Figure B.5 : XY strain data of ST37-650X650X3 panel configuration.

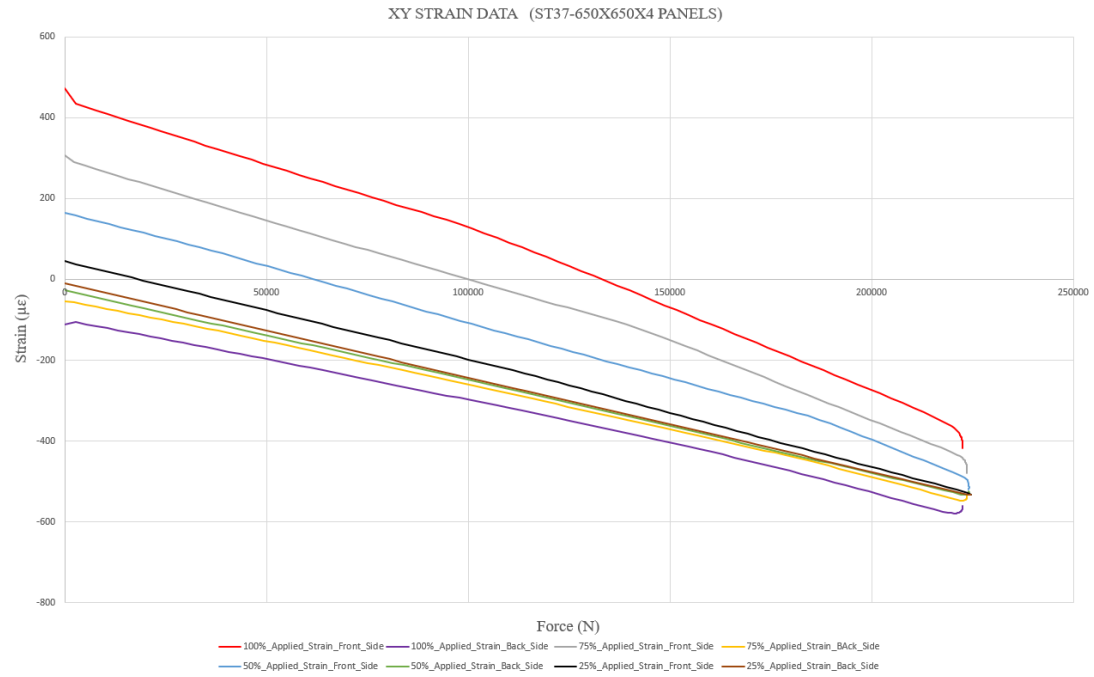

Figure B.6 : XY strain data of ST37-650X650X4 panel configuration.

CURRICULUM VITAE

Name Surname **: Taha Çimen**

EDUCATION **:**

- **B.Sc.** **:** 2022, Istanbul Technical University, Faculty of Mechanical Engineering

PROFESSIONAL EXPERIENCE AND REWARDS:

- 2022-Now: Structural Analysis Engineer at Turkish Aerospace Industry